Journal of Petroleum Science and Engineering 79 (2011) 65–85

Contents lists available at SciVerse ScienceDirect

Journal of Petroleum Science and Engineering

journal homepage: www.elsevier.com/locate/petrol

Multiphase flow behaviour during CO_2 geo-sequestration: Emphasis on the effect of cyclic CO_2–brine flooding

Ali Saeedi [a,*], Reza Rezaee [a], Brian Evans [a], Ben Clennell [b]

[a] Department of Petroleum Engineering, Curtin University, Western Australia, Australia
[b] Earth Science and Resource Engineering, CSIRO, Western Australia, Australia

ARTICLE INFO

Article history:
Received 25 February 2011
Accepted 26 July 2011
Available online 7 August 2011

Keywords:
CO_2 geo-sequestration
multiphase flow
cyclic injection
core-flooding

ABSTRACT

Geo-sequestration is considered to have a significant global potential for reducing the amount of anthropogenic greenhouse gas emissions, in particular carbon dioxide. In simple terms CO_2 geo-sequestration involves capturing the gas at its emitting source and then compressing and injecting it into a deep underground geological reservoir with a known seal where it will exist as a dense supercritical fluid. In this way the unwanted gas will be sequestered for perpetuity.

It is known that during many long term CO_2 geo-sequestration processes three will be parts of the underground reservoir subjected to cyclic CO_2–brine flooding. The multiphase flow characteristics of the fluids–rock system can change after each flooding cycle or in other words each flooding stage would be different from the other from the multiphase flow behaviour point of view. This continual change is due to various factors including: the capillary hysteresis effect, chemical reactions between the in-site created solute and the host formation rock, the effect of the stress applied to the reservoir and any formation damage or enhancements caused by the CO_2 or alternating CO_2–brine injection process. To the authors' knowledge there has not been an extended experimental study conducted to date on the effects of such cyclic flooding pattern on the multiphase flow characteristics of the system for more than two flooding cycles. This paper presents in details the equipment, procedure, protocol and the results of an experimental work carried out to understand the change in supercritical CO_2–brine–rock interactions subjected to this cyclic flooding pattern under in-situ reservoir conditions of pressure and temperature, with emphasis on change in multiphase flow characteristics of the system. The experiments were run on a number of sandstone samples with different permeability and porosity values to allow an evaluation of the change in experimental results with change in the sample properties. With this knowledge, we can better understand the significance of change in fluid flow characteristics during cyclic flooding which occurs in many CO_2 geo-sequestration processes in one form or the other.

1. Introduction

Due to the fact that during geo-sequestration CO_2 is injected to a relatively stationary body of brine saturating the target formation and also supercritical CO_2 has a density value which is an order of magnitude less than brine, apart from a limited area around the wellbore where CO_2 flows horizontally, it tends to flow upwards as it displaces the in-situ brine aside (Doughty and Pruess, 2004; Kumar et al., 2005; Nordbotten et al., 2005). This displacement could be classified as a drainage process during which the wetting brine phase is displaced by the non-wetting CO_2. This drainage process then could be followed by an imbibition process due to either or both of the flowing reasons:

- Alternating CO_2–brine injection: Similar to the Water-Alternating-Gas (WAG) scheme deployed for EOR purposes, in order to control the mobility and/or have better lateral dispersion of the injected CO_2, there could be a CO_2 injection period (drainage) followed by a period of brine injection (imbibition) behind the CO_2 front (Bennion and Bachu, 2006b; Emeka Eke et al., 2009). In this way CO_2 would be moving away from the well while being displaced by brine.
- Seasonal/periodic CO_2 injection: In certain environments a seasonal or periodic CO_2 injection may be required rather than a continuous injection. During such injection schemes, after cessation of the injection (drainage), the injected CO_2 flows away from the well in the form of free gas while being displaced by the in-situ brine (imbibition) and eventually moves upward due to buoyancy forces. This process can happen repeatedly as more periodic CO_2 injections are performed.

It is predictable that the multiphase flow characteristics of the fluids–rock system would change from one stage to another as it is

* Corresponding author at: 26 Dick Perry Avenue, Kensington, WA 6151, Australia. Tel.: +61 8 9266 4988; fax: +61 8 9266 7063.
E-mail address: Ali.Saeedi@Curtin.edu.au (A. Saeedi).

0920-4105/$ – see front matter © 2011 Elsevier B.V. All rights reserved.
doi:10.1016/j.petrol.2011.07.007

subjected to any of the described flooding schemes. These changes could occur due to any potential alteration to the petrophysical properties e.g. pore-network, porosity, permeability, etc., of the porous medium and/or the well-known capillary hysteresis (Juanes et al., 2006) as the cyclic flooding proceeds. A detailed investigation of the effect of such changes, using representative rock and fluid samples under in-situ reservoir P–T conditions, is vital before the commencement of any CO2 geo-sequestration project during which a cyclic CO_2–brine flooding is expected to occur. This would help to have a better understanding of the fate of the injected CO2, how the CO2 plume evolves and migrates through the porous medium and potential change in the CO2 injectivity into the target formation.

The produced experimental results in the literature to date on the multiphase flow characteristics of the fluids–rock system during CO_2 geo-sequestration do not extend beyond two successive injection cycles, including a primary drainage cycle followed by a subsequent imbibition cycle. The experiments conducted here include up to seven injection cycles (four drainage and three imbibition cycles). In addition to the core-flooding experiments there has been a number of other complementary measurements/analyses – such as NMR measurements, brine chemical analysis, etc. – carried out which have helped to more accurately understand and interpret the results achieved from the flooding tests.

2. Experimental measurements

2.1. Materials

2.1.1. Fluids

In total three main different types of fluids were used during the various stages of the experimental work conducted. These fluids included dead brine (brine with no dissolved gas content), CO_2-saturated brine (brine saturated with CO_2 at the in-situ reservoir P–T conditions) and water-saturated CO_2 (supercritical CO_2 saturated with water vapour at the in-situ reservoir P–T conditions). The CO_2 gas used was of a bottled high-purity grade (99.99%) carbon dioxide. The brine was prepared in the lab using demineralised water and appropriate amounts of analytical grade (99.95%) sodium chloride (NaCl).

2.1.2. Core samples

After shales with 46%, sandstones make up about 32% of all the sedimentary rocks, followed by carbonates with 22% (Leet and Judson, 1971). Therefore, deep sandstone aquifers are considered abundant in many sedimentary basins around the world and present a large storage capacity available for immediate CO_2 storage. The core samples used during this experimental work were all sandstone and were chosen from a number of varieties to cover a range of sandstone types present in such geological structures. The samples could be divided into four different groups based on their origin, porosity and permeability ranges and the type and degree of their clay content. Table 1 presents the properties of the core samples (either one standalone piece or composite). As can be seen from the table they cover a wide range of permeability values.

The samples in Group 1 were those drilled in both horizontal and vertical directions from the whole-cores taken from Well CRC-1 drilled into the Naylor Field of CO2CRC's Otway Basin Project (OBP) in early 2007. OBP has been the first CCS (carbon capture and storage) demonstration project undertaken in Australia with the main aim of demonstrating that CO_2 can be safely captured, transported and stored underground under Australian conditions (Sharma et al., 2009). Before being subjected to CO_2 injection in March 2008, the Naylor Field was a small depleted gas reservoir in the onshore Otway Basin in central southern Victoria, Australia (Knackstedt et al., 2010). In this field the Waarre Formation was the main hydrocarbon reservoir (Spencer et al., 2006). The core samples tested here were drilled from Unit C of this formation. Unit C rocks are made up of interbedded sandstone and claystone (Knackstedt et al., 2010) and the sandstones are generally quartz arenites, medium to coarse grained, fair to well sorted with characteristically high flow rates (Spencer et al., 2006).

The second group of samples were drilled from two separate quarried Berea Sandstone blocks purchased from Vermilion, Ohio in the United States. As requested from the supplier in the U.S., the two blocks were different from each other with respect to their absolute permeabilities. The Berea samples were characterised by clean, well-sorted and fine to medium grained sandstones with moderate to high permeability and moderate porosity values. The grains of the Berea sandstone consisted of predominantly quartz (85 to 90%) and feldspar (3 to 6%). The sand grains were cemented by quartz, dolomite (1 to 2%), clays (6 to 8%), and traces of iron sulphides. The rock samples in Group 3 were of Donnybrook Sandstone drilled from quarried blocks taken from the Donnybrook area in the South-west of Western Australia. These samples were of yellowish felspathic sandstone with a principal bonding of kaolin or halloysite and traces of iron oxide. As a general characteristic of the Donnybrook Sandstone, these samples were of low permeability and moderate porosity values. The fourth group of samples included a few short glauconitic sandstone samples. These samples were drilled in both horizontal and vertical directions from the whole-cores taken from an Australian offshore gas reservoir. The samples in this group were of moderate permeability and porosity values.

2.2. P–T conditions of the experiments

Table 2 lists the values of the in-situ reservoir condition parameters used during the experiments which were carried out under high pressure and temperature. The pressure, temperature and salinity values used were the same as the in-situ reservoir conditions of the Naylor Field of the Otway Basin Project (OBP). Unit C of Waarre

Table 1
Characteristics of the core samples used for the experiments.

Sample no.	Group no.	Sample ID	Length, cm	Diameter, cm	Lithology	Porosity, %	Permeability, mD
1	1	CO2CRC-1-V	9.79	3.88	Sandstone	20.01	751.1
2	1	CO2CRC-2,3-H[a]	9.18	3.89	Sandstone	17.31	788.3
3	1	CO2CRC-7-V	9.17	3.88	Sandstone	21.35	1899.6
4	1	CO2CRC-11,14-H[a]	8.23	3.88	Sandstone	22.03	3409.8
5	1	CO2CRC-36-V	8.62	3.88	Sandstone	17.26	108.2
6	1	CO2CRC-39,42-H[a]	9.1	3.87	Sandstone	15.49	252.6
7	2	BS-1-H	8.42	3.72	Sandstone	17.97	234.6
8	2	BS-2-H	8.46	3.73	Sandstone	18.4	141.13
9	2	BS-3-V	8.35	3.73	Sandstone	18.64	194.4
11	3	DB-1-H	7.18	3.81	Sandstone	16.01	14
12	3	DB-2-V	7.04	3.8	Sandstone	16.19	12.2
13	4	CL-40,68-H[a]	9.8	3.84	Sandstone	14.42	123.5

[a] Composite core samples i.e. the core sample is made up of two separate short core-plugs.

Table 2
Reservoir P–T conditions during the experimental work (when applicable).

Reservoir parameter	Value
Pore pressure (psi)	2580.0
Overburden pressure (psi)	6725
Reservoir temperature (°C)	83
Formation water salinity (ppm NaCl)	20,000

Formation in the Naylor Field, which has been the target for the first phase of CO_2 injection, is located at a depth of about 2050 m. This is the depth that all the core samples tested came or assumed to have come from.

2.3. Experimental work

2.3.1. Experimental apparatus

The core-flooding experiments were carried out using the high pressure–high temperature, three-phase steady-state core-flooding apparatus located within the Department of Petroleum Engineering at Curtin University. A schematic of the core-flooding rig is presented in Fig. 1. The apparatus is capable of handling experiments with pressures up to 15,000 psi and temperatures up to 200 °C. The critical wetted metal parts of the apparatus are made of highly corrosion resistant material e.g. hastelloy, titanium or duplex and super duplex stainless steel, which make the equipment rust free and corrosion resistant even under high temperature environments with high chloride concentrations. All the components carrying fluids during experiments are placed inside a large constant temperature convection oven (Fig. 1). The temperature inside the oven is controlled using a PID (proportional–integral–derivative) controller module which can regulate the temperature with an accuracy of 0.2 °C. The oven is also equipped with three fans, which help to circulate the hot air inside it ensuring that the temperature remains the same at every point inside the oven.

The core-flooding apparatus utilises four injection pumps (Fig. 1) which could be run either independently or in synchronised pairs. All four pumps are of pulsation-free, positive-displacement pump type and each offer an injection capacity of 300 cm^3 in one injection cycle. They can inject the fluids under various injection scenarios of constant flow-rate, constant pressure, constant pressure with adjustable pressure ramp and reaching a target injection volume. All four pumps could be operated directly using the keypads placed in front of them or using the monitoring/controlling software installed on two PCs connected to the apparatus. In the injection pumps the pressure, volume and flow-rate values can be set and recorded with accuracies of 2 psi, 0.05 cm^3 and 0.05 cm^3/h respectively. All the pressure sensors utilised within the core-flooding rig have the same 2 psi measurement accuracy.

The fluid sample bottles (Fig. 1) each have a capacity of 1500 cm^3 which, when combined with the ability of the injection pumps to operate in synchronised pairs, can provide enough injection capacity to reach steady-state conditions even in low permeability samples. The core-holder used during this research was a standard biaxial core-holder (Fig. 2). Standard biaxial or hydrostatic type core-holders are defined as core-holders that have common radial and axial pressures applied to the core-sample. A specially designed spider-web-type groove pattern (Fig. 2) is utilised on the end-faces of the core-holder's distribution plugs which come in contact with end-faces of the core sample. This is to make sure that the fluids, before entering or on exiting the core-sample, are evenly distributed on the whole face of the core-sample. This type of groove pattern is very effective in

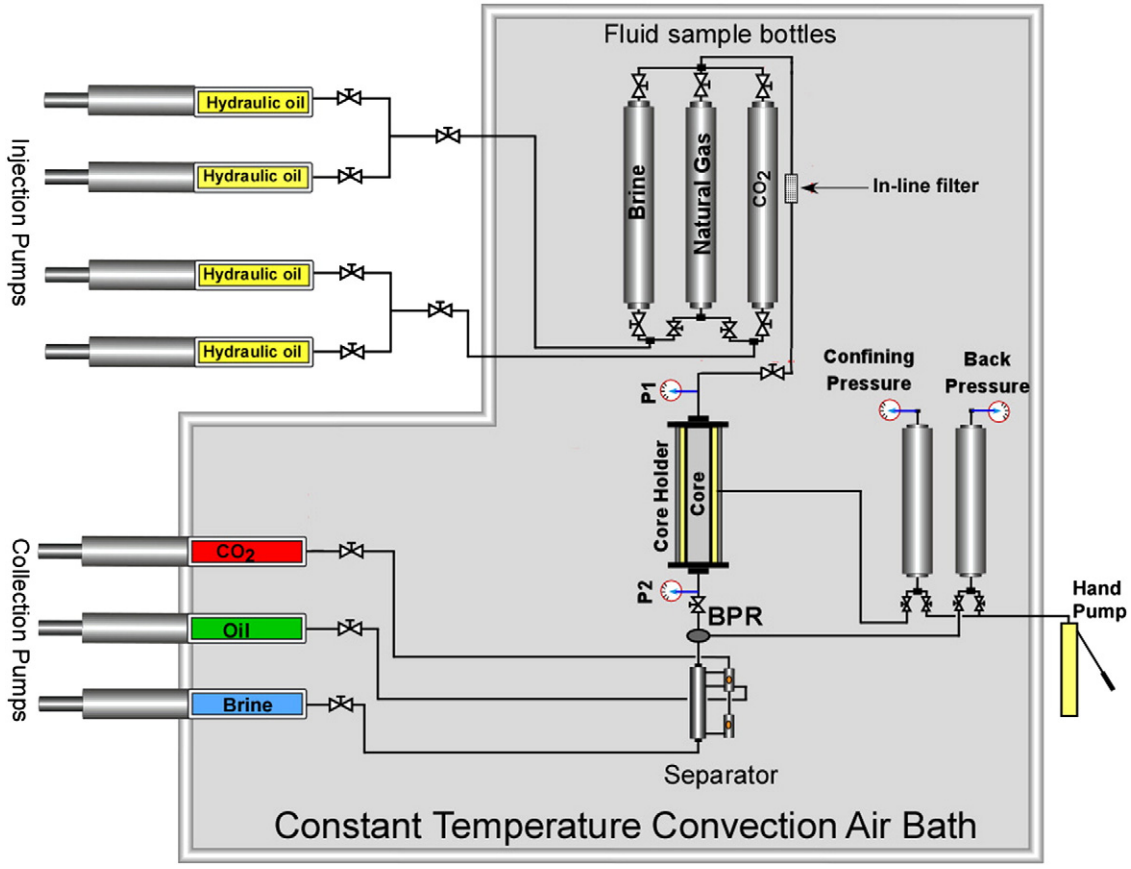

Fig. 1. The schematic diagram of the experimental apparatus used to run the core-flooding experiments.

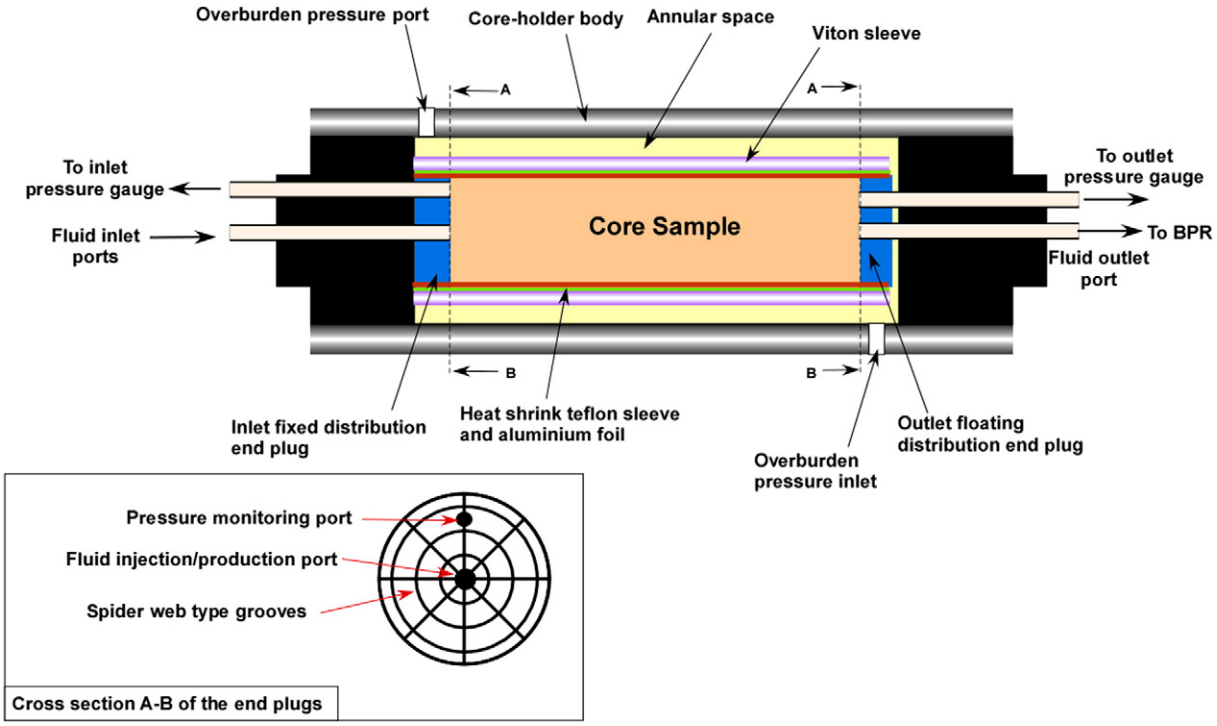

Fig. 2. Schematic cross-sectional illustration of the configuration of the core-holder assembly used during core-flooding experiments.

making the capillary inlet and outlet effects, which are commonly experienced during the displacement experiments, less pronounced. All core-holder out-flow fluids are passed through a dome-type back-pressure regulator (BPR) which keeps the pressure inside the sample constant and equal to reservoir in-situ pore pressure and prevents any back-flow of the produced fluids into the core-sample.

The separation and collection system comprises of a high pressure–high temperature three-phase vertical separator, three collection pumps and associated sensors. The separation occurs due to gravity inside the specially designed separator, which can operate at the same pressure and temperature as reservoir in-situ conditions i.e. P–T conditions inside the core sample. This is highly beneficial, especially for the material balance calculations, since there is no need to back-convert the produced volumes to reservoir conditions, which would be necessary if the fluids were being flushed into ambient conditions. Furthermore, for the experiments conducted during this research, the high pressure inside the separator eliminated the evolution of the CO_2 already dissolved in the CO_2-saturated injection brine or the evaporation of the hot water coming out of the core-sample, both of which could cause serious errors during the material balance calculations. With regards to technical specifications, the three collection pumps are identical to the injection pumps described before.

All of the sensors and electronic interfaces of the apparatus are connected to two computers with appropriate data logging and monitoring software installed on both. The whole system including the sensors, the PID controllers and the injection and collection pumps are monitored and controlled using these two computers. The data logging can be done with time-steps as short as one second.

2.3.2. Experimental procedure

It is a normal practise in the industry that if the lengths of the individual core-plugs are short they are stacked together for each particular flow unit to form composite core samples (Langaas et al., 1998). This is done to satisfy the scaling factor defined by Rapoport and Leas (1953) through making longer samples which when coupled

Table 3
Summary of the cyclic CO_2–brine flooding tests conducted on various samples.

Test no.	Sample name	Pore vol, cm^3	k, mD	CO_2 inj. flow-rate, cm^3/h	Water inj. flow-rate, cm^3/h	Capillary number, Nc	Rapoport scaling coefficient
1	CO2CRC-1-V	23.213	751.10	300	250	8.93E-05	0.157
2	CO2CRC-2,3-H	18.859	788.30	300	250	8.88E-05	0.147
3	CO2CRC-7-V	23.1	1899.60	300	300	8.93E-05	0.147
4	CO2CRC-11,14-H	21.5	3409.80	300	300	8.93E-05	0.132
5	CO2CRC-36-V	17.564	108.22	250	200	7.44E-05	0.115
6	CO2CRC-39,42-H	16.49	252.60	250	200	7.48E-05	0.122
7	BS-1-H	16.476	234.60	300	200	9.71E-05	0.147
8	BS-2-H	16.975	141.13	300	200	9.66E-05	0.147
9	BS-2-H	16.975	141.13	120	100	3.86E-05	0.059
10	BS-3-V	17.002	194.36	300	200	9.66E-05	0.145
11	DB-1-H	13.135	14.00	150	100	4.63E-05	0.060
12	DB-1-H	13.135	14.00	200	150	6.17E-05	0.080
13	DB-2-V	12.894	12.20	150	100	4.65E-05	0.059
14	CL-40,68-H	16.725	123.50	300	200	9.11E-05	0.161

Table 4
End-point brine saturation at the end of each injection cycle during the cyclic CO_2–brine injection experiments.

Test no.	Sample name	End-point brine saturation, %						
		1st Drain.	1st Imb.	2nd Drain.	2nd Imb.	3rd Drain.	3rd Imb.	4th Drain.
1	CO2CRC-1-V	44.7	82.2	46.1	82.2	45.6	82.5	44.6
2	CO2CRC-2,3-H	50.1	80.4	51.2	80.3	50.8	80.7	51.1
3	CO2CRC-7-V	46.9	90.6	46.4	91.2	45.8	90.2	46.3
4	CO2CRC-11,14-H	52.4	91.0	52.3	88.8	51.2	90.3	50.2
5	CO2CRC-36-V	50.8	79.1	51.5	78.9	52.2	79.0	50.4
6	CO2CRC-39,42-H	54.6	80.2	–	–	–	–	–
7	BS-1-H	44.9	78.5	44.7	79.0	44.1	78.8	44.8
8	BS-2-H	44.8	80.6	44.0	80.4	44.4	81.1	44.9
9	BS-2-H	49.5	81.4	49.4	81.3	49.4	81.3	49.3
10	BS-3-V	45.8	76.5	45.1	76.4	45.4	76.7	45.6
11	DB-1-H	60.5	73.2	58.4	71.4	57.7	72.2	57.9
12	DB-1-H	59.0	73.8	–	–	–	–	–
13	DB-2-V	64.6	71.8	–	–	–	–	–
14	CL-40,68-H	51.9	78.1	48.2	78.7	48.4	79.2	49.2

by high enough flow-rates, would make the occurrence of any possible end-effect during the tests less pronounced. Some of the tested samples in this work are made using this technique. To insure that there is no capillary discontinuity between the stacked short plugs, two layers of lint-free tissues were placed between polished end-faces of the plugs as it is recommended in various literatures (Osoba et al., 1951; Hinkley and Davis, 1986; Zekri and Almehaideb, 2006).

For the core-flooding experiments conducted during this research, a special multilayer combination sleeve was used. This combination sleeve was necessary due to the tendency of CO_2 to diffuse and penetrate through most flexible rubber sleeves which firstly could cause the sleeve to lose its integrity and fail. Secondly, due to loss of CO_2 through diffusion, the material balance calculations for each individual experiment, which was necessary to work out the residual saturations inside the core-sample, would not add up. This combination sleeve was made of three layers including one layer of heat-shrink Teflon sleeve, one layer of aluminium foil and one layer of conventional Viton sleeve. The heat-shrink Teflon sleeve had an extremely low permeability to CO_2, however, to make sure that the CO_2 would not escape to the overburden annular space, a layer of aluminium foil was also placed between the Teflon and the Viton sleeve.

Below is an outline of the steps involved in carrying out each experiment:

1. Core sample preparation and preliminary measurements:
   1.1 The 1.5″ (3.81 cm) diameter core-plugs were cut from whole cores or blocks of outcrop rocks. The core-plugs were cut using air to avoid any possible damage to the samples caused by using water or any other fluid as the drilling fluid. Whenever possible, it was tried to recover long enough samples to avoid using composite cores. Those intervals were chosen for coring which had no or little heterogeneity.
   1.2 After drying the samples in a vented oven under 60 °C for 72 h, the porosity and permeability measurements were carried out using an automated helium porosi-permeameter under full reservoir in-situ effective pressure.
   1.3 After saturating the samples and ageing them in the synthetic formation brine for two weeks, the NMR measurements were performed on a number of samples using a Resonance Instruments Maran-Ultra 2 MHz bench-top spectrometer.
2. Core-flooding procedure:
   2.1 The samples were wrapped in the previously described multi-layered sleeve before being inserted into the core-holder. In order to eliminate the effect of gravity segregation (underrun or override of the injected fluids) within the sample while undergoing the core-flooding experiments, the core-holder containing the sample was placed vertically and injection was performed from base to the top. After loading the wrapped sample into the core-holder, using a hand pump, the overburden fluid was pumped into the annular space between the outer diameter of Viton sleeve and the inner surface of the core-holder shell. The injection of overburden fluid was

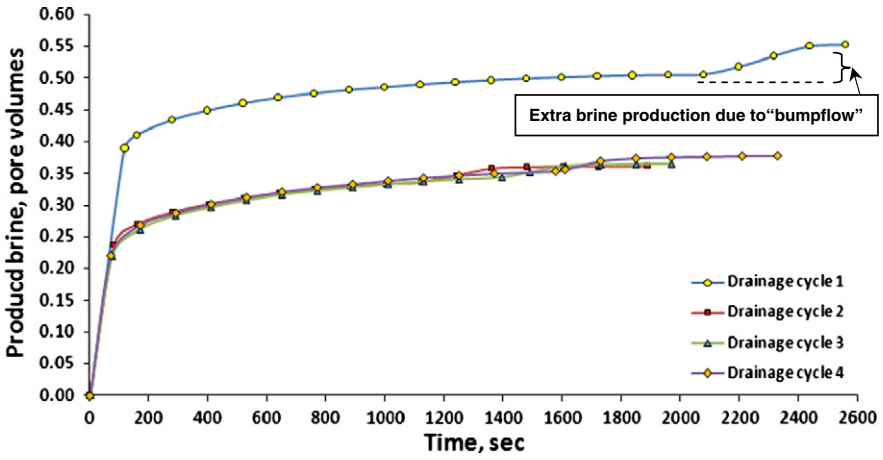

Fig. 3. Brine production versus time for the four drainage cycles conducted in test number 1 on Sample CO2CRC-1-V (k = 751.1 mD, Ø = 20.01%).

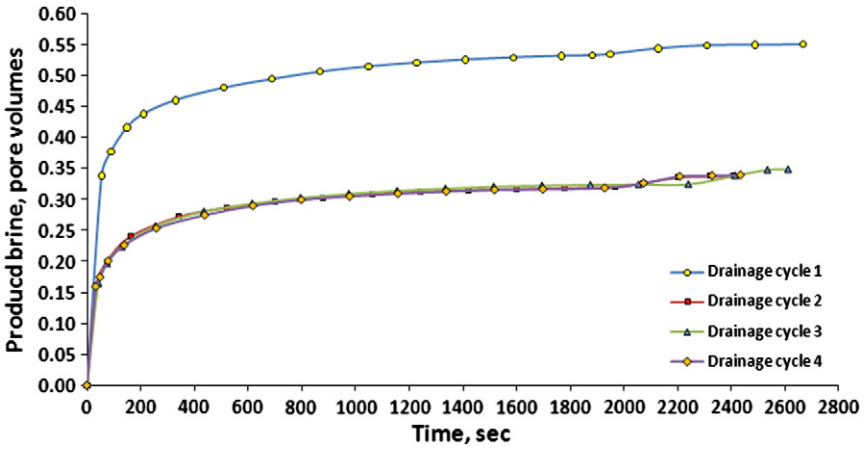

Fig. 4. Brine production versus time for the four drainage cycles conducted in test number 7 on Sample BS-1-H (k = 234.6 mD, Ø = 17.97%).

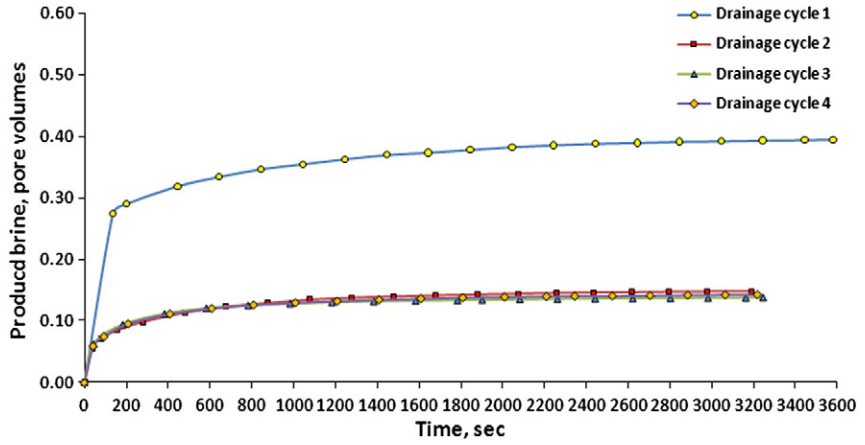

Fig. 5. Brine production versus time for the four drainage cycles conducted in test number 11 on Sample DB-1-H (k = 14 mD, Ø = 16.01%, CO_2 inj. flow-rate = 150 cm^3/h).

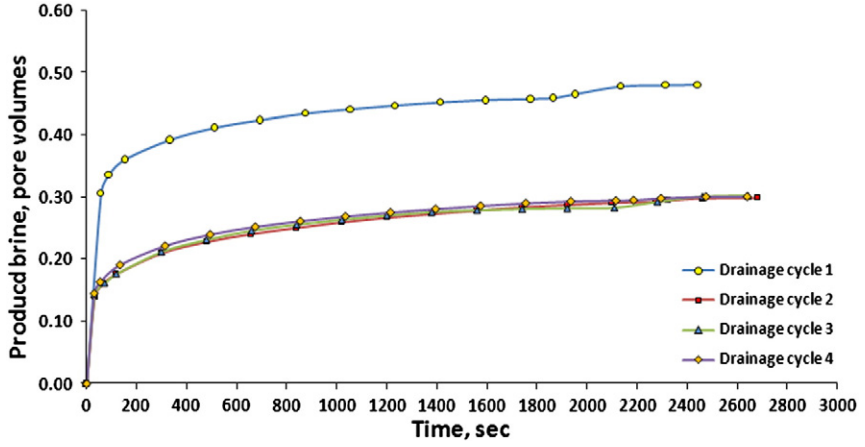

Fig. 6. Brine production versus time for the four drainage cycles conducted in test number 14 on Sample CL40,68-H (k = 123.5 mD, Ø = 14.42%).

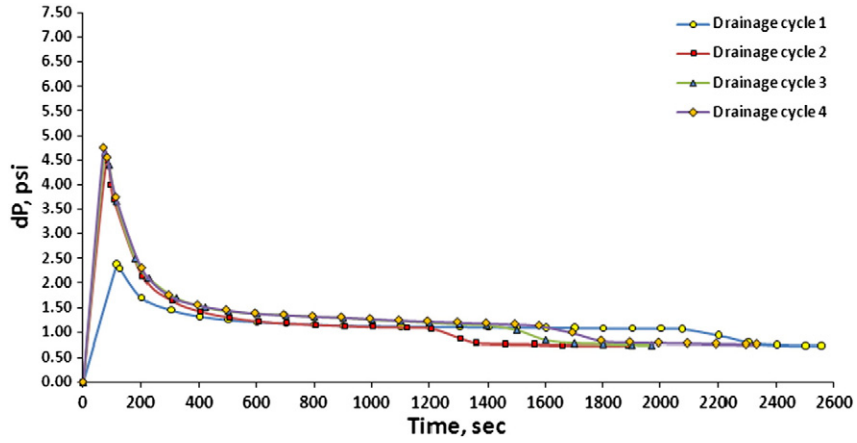

Fig. 7. Differential pressure across the sample versus time for the four drainage cycles conducted in test number 1 on Sample CO2CRC-1-V (k = 751.1 mD, Ø = 20.01%).

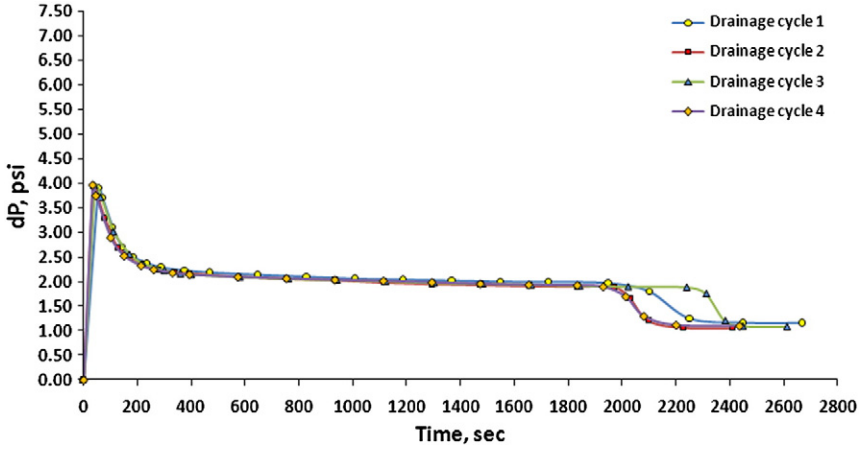

Fig. 8. Differential pressure across the sample versus time for the four drainage cycles conducted in test number 7 on Sample BS-1-H (k = 234.6 mD, Ø = 17.97%).

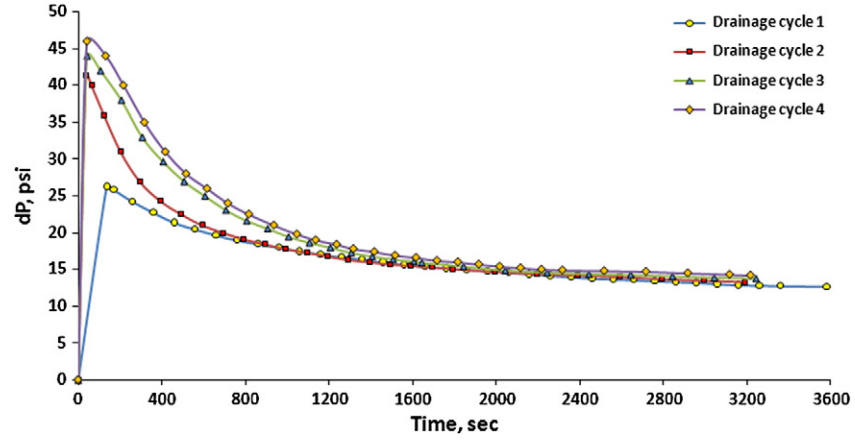

Fig. 9. Differential pressure across the sample versus time for the four drainage cycles conducted in test number 11 on Sample DB-1-H (k = 14 mD, Ø = 16.01%, CO_2 inj. flow-rate = 150 cm^3/h).

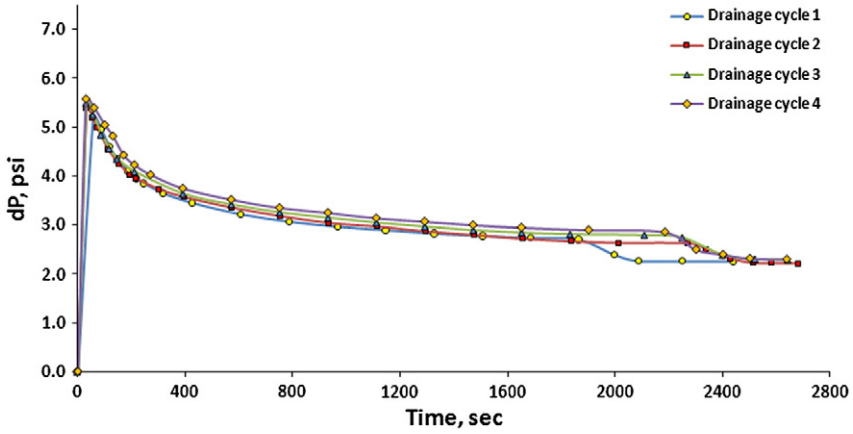

Fig. 10. Differential pressure across the sample versus time for the four drainage cycles conducted in test number 14 on Sample CL-40,68-H (k = 123.5 mD, Ø = 14.42%).

performed from the lower overburden pressure port displacing and expelling the air in the annular space from the top port.

2.2 After gradually increasing the overburden pressure to the full reservoir net effective pressure, all the inlet and outlet ports of the core-holder were capped or connected to appropriate flow-lines and pressure gauges. Then low pressure (~300 psi) CO_2 gas was passed through the sample for at least 20 min. Due to its high diffusivity, CO_2 would displace and replace any air trapped in the sample pores. Compared to air, the CO_2 which replaced the air could be evacuated from the sample more effectively when required. Furthermore, any remaining CO_2 after evacuation would readily dissolve in the saturating dead brine and removed from the sample during the later in-situ saturation process.

2.3 After flushing the sample by CO_2, all the flow-lines and the sample inside the core-holder were evacuated using a vacuum pump for at least 24 h. Then the Back pressure was brought to full reservoir in-situ pressure, and the air bath temperature also was raised to reservoir temperature. Then the core sample was displaced and saturated using dead formation brine while the confining pressure was increased and then maintained equal to its in-situ reservoir value. The sample was left under reservoir conditions in contact with brine for another 48 h to become completely saturated with dead brine and to establish adsorption equilibrium.

2.4 In the next step the CO_2-saturated brine was injected into the core sample at constant flow-rate to displace the dead formation brine. The CO_2-saturated brine injection continued until steady-state conditions were achieved i.e. constant and steady differential pressure across the sample and production flow-rate equal to injection flow-rate.

2.5 The injection of the vapour-saturated CO_2 began at constant flow-rate (drainage). The displacement continued until steady-state conditions were reached i.e. no more brine production and constant and steady differential pressure across the sample. At the conclusion of this drainage process there was a so called 'bump flow' i.e. a short period of high injection flow-rate, performed to examine and quantify the existence of capillary end-effect (Rapoport and Leas, 1953; Heaviside and Black, 1983; Grigg and Svec, 2006).

2.6 To investigate the effect of cyclic CO_2–brine flooding, after the completion of the above-described drainage process, all the experiments would normally continue with several subsequent cycles of imbibition and drainage stages using CO_2-saturated formation brine and vapour-saturated CO_2 respectively as the displacing fluids.

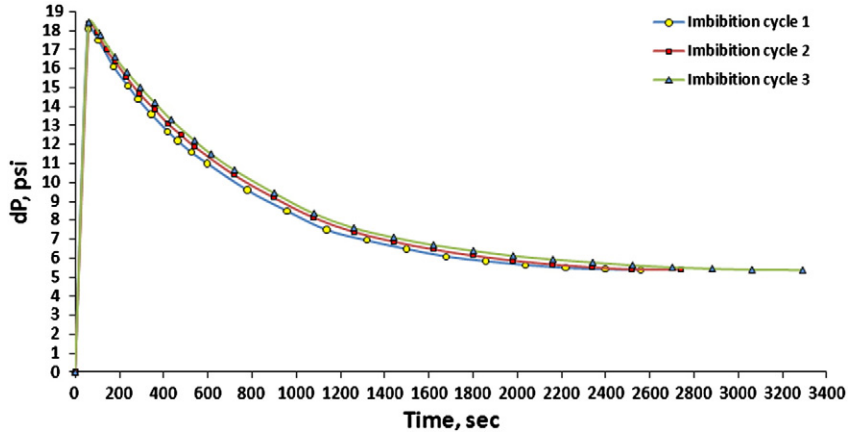

Fig. 11. Differential pressure across the sample versus time for the three imbibition cycles conducted in test number 5 on Sample CO2CRC-36-V (k = 108.2 mD, Ø = 17.26%).

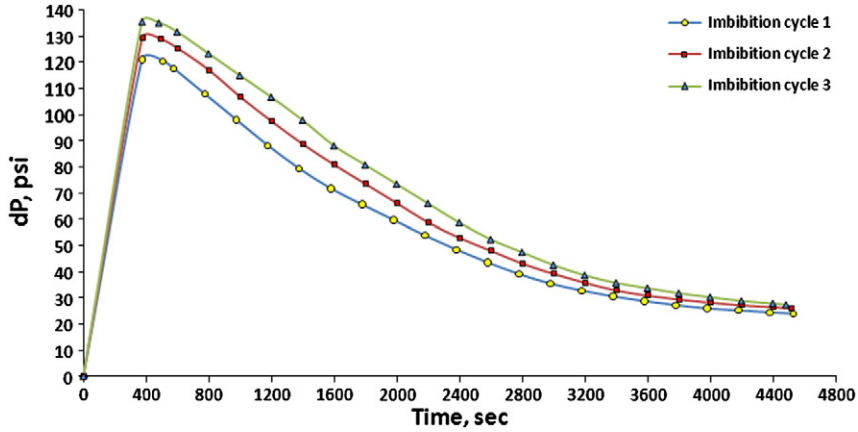

Fig. 12. Differential pressure across the sample versus time for the three imbibition cycles conducted in test number 11 on Sample DB-1-H (k = 14 mD, Ø = 16.01%, CO_2 inj. flow-rate = 200 cm^3/h).

During all the flooding procedures explained, all the system pressures, volumes and flow-rates were being recorded digitally using two computer machines.

Due to the viscosity and density contrast between supercritical CO_2 and brine, any long time lag between the end of one injection cycle and the start of the next could distort the stabilised and uniform saturation profile achieved at the end of the first cycle. Therefore, for each sample, as many injection cycles as possible were performed non-stop in one day only. During each injection cycle on average about 12 pore volumes of CO_2 or brine were passed through the core sample before stabilised conditions i.e. no more production of the displaced phase and constant and stable pressure drop across the sample, were reached.

After the completion of the core-flooding experiments, each sample underwent a second series of dimension, porosity and NMR measurements. These complementary measurements were performed to detect any possible physical changes (e.g. alteration to the pore size distribution of the sample), which could had occurred during the flooding process. In addition, in order to determine if there had been any chemical reaction between the injection fluids and the samples, two chemical composition analyses were conducted on a few brine samples taken from both injection and production sides of the core samples during the flooding process. The results of these complementary measurements/analyses would help also to better understand and interpret the results of the flooding experiments conducted which constitute the main part of this research.

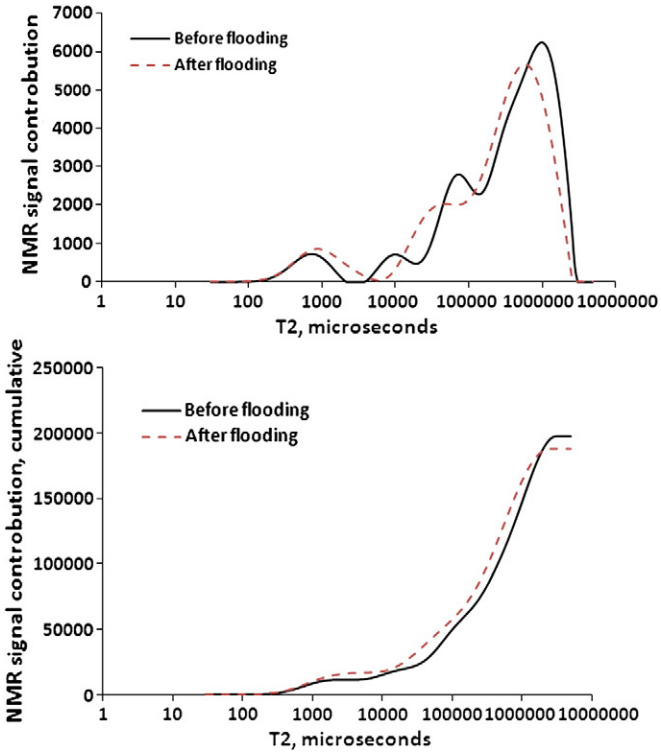

Fig. 13. Change in the incremental (top) and cumulative (bottom) T2 distribution of Sample CO2CRC-2-H after undergoing cyclic CO_2–brine injection.

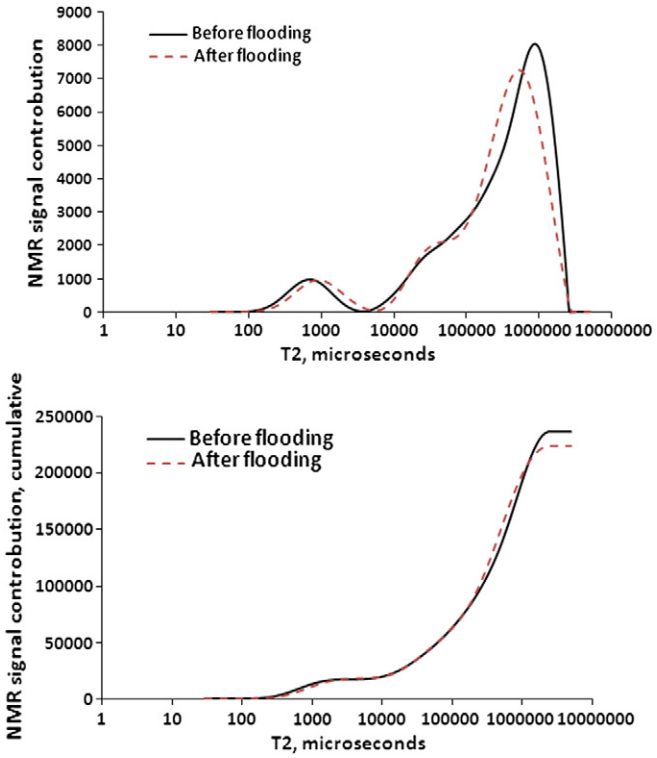

Fig. 14. Change in the incremental (top) and cumulative (bottom) T2 distribution of Sample CO2CRC-3-H after undergoing cyclic CO_2–brine injection.

2.3.3. Experimental results

2.3.3.1. Core-flooding experiments. In total, 14 experiments were conducted with the specific focus of investigating the effect of cyclic CO_2–brine injection on the multiphase flow behaviour of the fluids–rock system during underground CO_2 disposal.

In addition to providing some general information about each experiment conducted and the end-point brine saturations for each injection cycle, presented here are the results of the brine production and differential pressure across the sample, all versus time, for one representative sample from each sample group. The brine production and differential pressure profiles are provided for each individual injection cycle performed on each sample. Due to the fact that supercritical CO_2 has a much lower viscosity than brine, the cycles involving displacement of CO_2 by brine (imbibition) were of highly favourable mobility ratio (M) i.e. $(M) \ll 1$, and as a result very little amounts of CO_2 were produced after the brine breakthrough (BT). Therefore, the fluid production profiles are presented for the drainage cycles only. It is worth noting that the actual raw experimental data were recorded for every second using the monitoring/controlling software of the core-flooding apparatus. However, the graphs presented here show the data which were fitted to the raw data with approximately 1–3 minute time intervals between two successive data points. The size of the time intervals depended on the total duration of each experiment i.e. the longer the total duration of the experiment, the longer the time intervals between the data points of the fitted data.

Listed in Table 3 are the values of a number of important sample and experimental condition parameters. In real life in an underground CO_2 storage medium, apart from the portion of the reservoir in the vicinity of the wellbore, the displacement velocity would be low and the flow would be highly dominated by capillary forces. As mentioned before, in laboratory flooding experiments, however, in order to avoid the adverse effects of the well-defined capillary end-effect and have a uniform displacement, the flow-rates need to be sufficiently high. In order to investigate the effect of change in the flow-rate on the multiphase flow characteristics during the cyclic CO_2–brine injection, as can be seen from Table 3, a few experiments also were run under varying injection flow-rates.

Table 4 lists the end-point brine saturations obtained at the end of the injection cycles performed during all 14 cyclic CO_2–brine flooding experiments conducted on various samples. As can be seen from the table, for three experiments the end-point brine saturations are reported for the first drainage and first imbibition cycles only. This is because either a hardware failure occurred during running the experiment or the recorded brine production data for the rest of the cycles were not of reliable quality to be analysed and reported.

Figs. 3 to 6 present the brine production profiles observed at the outlet face of the core-plugs for four samples (one sample per each sample group). Each figure shows the brine productions versus time for all drainage cycles performed on a sample. As discussed earlier, a short period of so called “bump flow” was carried out at the conclusion of each cycle. This was necessary, especially in moderate to high permeability samples to establish true end-point saturations and remove any potential anomalous brine hold-up, which may have been created at the outlet of the sample due to the well-characterised capillary end-effect phenomenon. As can be seen in some of the graphs plotted, for the majority of the experiments conducted, abrupt increase in brine production close to the end of each injection cycle due to the “bump flow”, confirmed the existence of such saturation anomalies.

Figs. 7 to 10 present the differential pressures across the sample versus time for the experiments whose brine production profiles were reported before. In addition to the drainage cycles, the differential pressure profiles during imbibition cycles are also presented for two samples of CO2CRC-36-V and DB-1-H in Figs. 11 and 12 for comparison purposes. The differential pressure data for all the drainage or imbibition cycles are displayed for each sample in one single graph. The majority of the resulted differential pressure profiles for the drainage cycles show a sudden, steep decline close to their conclusion. These abrupt declines were due to the removal of the anomalous brine saturation caused by the

capillary end-effect through conducting the previously described "bump flow".

2.3.3.2. NMR measurements. Nuclear Magnetic Resonance refers to the response of atomic nuclei of hydrogen when it is immersed in a static magnetic field and exposed to a second oscillating one. Response of the NMR relaxation measurements can be used to extract useful petrophysical information such as irreducible bulk volume (BVI), clay-bound water volume (CBW), and movable bulk volume (BVM). This allows defining effective porosity, total porosity, and permeability index (Coates et al., 1999).

Among others, the properties of the fluids contained in the pore space of a porous medium which influence the data obtained from the NMR measurements are longitudinal relaxation time (T1), transverse relaxation time (T2). T1 is a measure of how fast the protons in the fluid exposed to the external magnetic field relax longitudinally (relative to the axis of the static magnetic field). T2 is an indication of how fast the protons relax transversely (again relative to the axis of the static magnetic field) (Coates et al., 1999). T2 relaxation time depends on many parameters such pore fluid type, mineralogy and pore sizes. Among these, when dealing with the same rock type and the same pore filling fluid, pore size is the most important parameter that controls T2 relaxation time. There is a direct relationship between pore size and T2. As pore size of a porous media increases it takes more time for hydrogen nuclei to relax thus T2 will increase. Whereas for rocks with small pore sizes T2 relaxation time shift toward smaller values.

As mentioned earlier, a Resonance Instruments Maran-Ultra 2 MHz bench-top spectrometer (operating at a frequency of 1.92 MHz) was used to carry out the NMR measurements. The NMR tests were conducted on a number of the samples used during the core-flooding tests. For most of these samples NMR measurements were carried out twice, once before and once again after they underwent the cyclic flooding experiments. A hard pulse CPMG (Carr–Purcell–Meiboom–Gill) sequence was used to generate the T2 relaxation spectrum on the samples tested.

An NMR test (CPMG sequence) was also conducted on a 15 ml NiCl solution sample prepared by dissolving NiCl in demineralised water. The initial amplitude (or cumulative T2 distribution) recorded for this 15 ml solution sample can be used later in conjunction with the initial amplitude (or cumulative T2 distribution) recorded for the core samples tested afterwards to evaluate their NMR porosity. The solution sample was used also, as required on several occasions, to calibrate the NMR instrument using the FID (Free Induction Decay) acquisition sequence.

Figs. 13 and 14 present the incremental and cumulative T2 distributions for samples CO2CRC-2-H and CO2CRC-3-H (stacked together to make up composite sample CO2CRC-2,3-H) acquired by conducting NMR measurements on them before and after they underwent the cyclic flooding procedure. Fig. 15 also presents the same data for sample DB-1-H. It is worth noting that, as explained earlier, since all samples were fully saturated with formation brine prior to the NMR measurements, the incremental T2 distribution for each sample represents its relative pore size distribution.

2.3.3.3. Other complementary measurements. After carrying out the cyclic flooding tests on the core samples, a second set of porosity measurements was conducted on a number of the core samples. Two chemical composition analyses were also performed on the brine used during the core-flooding experiments. One of the brine samples was taken from the original brine before being injected through the core samples and the other sample was a mixture of several brine samples taken from the produced brine on the outlet side of a few samples including two Berea and two samples from the CO2CRC's Naylor Field. Table 5 presents the dimension and porosity measurements conducted on a number of core samples after the completion of the core-flooding experiments.

Table 6 has been constructed using the results of the two brine chemical composition analyses mentioned earlier. The third column

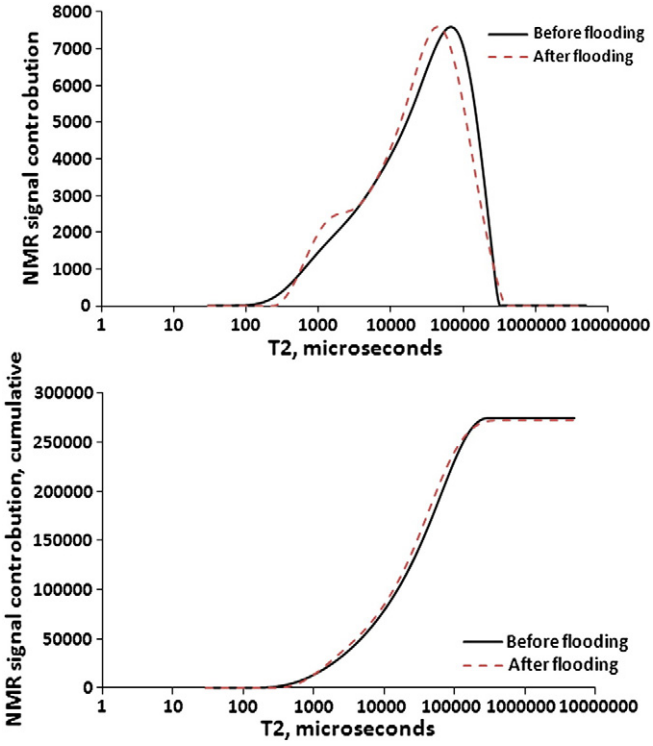

Fig. 15. Change in the incremental (top) and cumulative (bottom) T2 distribution of Sample DB-1-H after undergoing cyclic CO_2–brine injection.

Table 5
Porosity and dimension measurement results for a number of the core samples after performing the flooding experiments on them.

No.	Group no.	Sample ID	Length, cm	Diameter, cm	Porosity, %
2	1	CO2CRC-2,3-H[a]	9.14	3.88	17.18
4	1	CO2CRC-11,14-H[a]	8.17	3.87	21.84
5	1	CO2CRC-36-V	8.57	3.86	17.1
7	2	BS-1-H	8.42	3.72	17.85
13	4	CL-40,68-H[a]	9.77	3.83	14.33

[a] Composite core samples.

Table 6
Increase in the concentration of a number of chemical elements in the brine after being injected through the samples.

Chemical species	Unit	Amount of increase after the test
Bicarbonate as $CaCO_3$	mg/l	480
Calcium-filterable	mg/l	123
Carbonate as $CaCO_3$	mg/l	<1
Magnesium-filterable	mg/l	37
Potassium-filterable	mg/l	1

of this table shows the amount of increase in the concentration of a few chemical species, which could potentially have originated from the possible chemical reactions between the rock and the fluids during the flooding experiments.

3. Interpretation and analysis

Fig. 16 is a cross-plot showing the typical relationship between the porosity and permeability values of the core samples. It is apparent from this figure and as generally one may expect, the lowest porosities belong to the lowest permeable samples and the highest ones belong to the samples which have the highest permeabilities. The porosity data plotted here, which were obtained using a helium porosimeter, match well with those calculated for a few samples from the NMR measurements (Table 7). It is worth noting that, as is the case here, the NMR measurements normally overestimate the porosity values. This is because NMR detects all water contained in all the pores including the clay-bound-water, which is not normally removed during the drying procedure. This clay porosity, however, does not contribute to the effective porosity values measured using helium.

Using the data generated during the various experimental work carried out, in addition to some general discussions on the multiphase flow characteristics of the fluids–rock system pertaining to CO_2 geo-sequestration, in the following section of the paper it has been tried to determine if there has been any alteration in these characteristics as a result of the cyclic CO_2–brine flooding pattern.

3.1. Effect of cyclic CO_2–brine flooding on the saturation profiles

3.1.1. Drainage cycles

Fig. 17 shows the end-point residual brine saturation data for the total of four drainage cycles performed on various samples. With regards to the effect of the cyclic injection on the production profiles or the end-point saturations, as can be seen from this figure, apart from a number of slight variations, overall there is no significant or consistent trend apparent among the data. The saturation data for experiment numbers 6, 9, 12 and 13 are not included in this plot. Experiments number 9 and 12 were run for sensitivity analysis only and Experiments 6 and 13 only produced quality saturation data during their first drainage cycles. As stated above, it seems that the saturation data from one cycle to the other were not affected by the cyclic flooding process; however, there are a number of points, which need to be discussed about the saturation data for each individual drainage cycle. A number of the following discussions are presented on the saturation data for the first drainage cycle only but since all drainage cycles produced fairly similar results, they can be extended to the rest of three drainage cycles.

It can be seen from the saturation data reported in Table 4 that the brine residual saturations achieved at the end of all the drainage cycles are relatively high. The high end-point residual brine saturations observed here can also be seen within the limited experimental results reported by other researchers (Bennion and Bachu, 2005, 2006b, 2007, 2010; Perrin et al., 2009). These high residual saturations can be explained using the concepts of mobility ratio and interfacial tension (IFT). First of all, the highly unfavourable mobility ratio, caused by high brine to supercritical CO_2 viscosity ratio, dominates the flooding experiments causing highly non-uniform displacement of brine by CO_2 (Bennion and Bachu, 2006a; Espinoza and Santamarina, 2010) characterised by highly pronounced end-effects. For instance, the brine to CO_2 viscosity ratio under the P–T conditions of the experiments run here was about 10.

Secondly, since IFT of the CO_2–brine system is very low, as will be explained later, during a drainage cycle, premature CO_2 breakthrough can severely influence the displacement of the wetting phase i.e. brine. Based on the theory behind EOR, and as has been confirmed through numerous experimental, simulation and field studies, through reduction in the IFT between the wetting (normally brine) and non-wetting phase (normally hydrocarbon), the trapped non-wetting phase can become mobilised again and move through the pore-throats and be produced (Pope and Baviere, 1991). This occurs because reducing the IFT would reduce the capillary pressure at the pore-throat resisting the passage of the non-wetting phase from one pore to the next, towards the production side of the porous medium. But such EOR processes are classified as imbibition or imbibition-like displacements, during which the saturation of the non-wetting hydrocarbon phase is

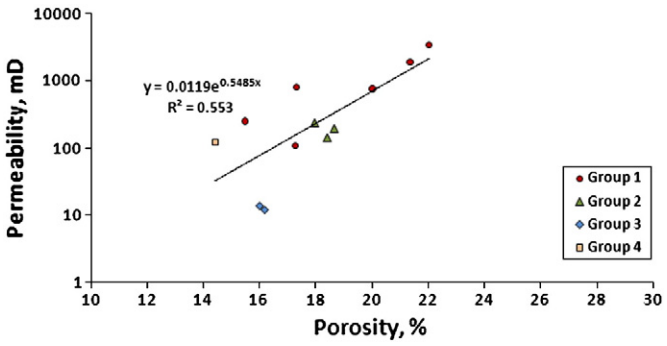

Fig. 16. Porosity-permeability relationship for various samples within different groups.

Table 7
Comparison between the NMR and helium porosity values for a number of samples used.

Sample ID	NMR porosity, %	Helium porosity, %
CO2CRC-2,3-H	21.1	17.31
CO2CRC-11,14-H	23.7	22.03
BS-1-H	18.2	17.97
DB-1-H	17.9	16.01

reduced. The displacement of brine by CO_2, however, is a drainage process and as explained below, low IFT, in fact, can reduce the displacement efficiency.

During such drainage processes as CO_2 displacing the brine, if the IFT value is low, the capillary pressure at the pore-throat is also low and the pressure in the non-wetting phase does not need to rise to high values to be able to overcome the capillary pressure and pass through the pore-throat (Craig, 1975; Dullien, 1992). In other words, once CO_2 enters a pore-body, soon afterwards, under the influence of unfavourable mobility, it would preferentially channel through the centre of the pore-body, which is filled with much higher viscosity brine, and quickly pass through the downstream pore-throat. This reduces the amount of brine which could be produced ahead of the invading CO_2. This phenomenon causes premature CO_2 breakthrough and eventually, coupled with non-uniform displacement, reduces the overall brine recovery, resulting in high residual brine saturations. This is contrary to the conclusion made by Bennion and Bachu (2006a) but at the same time in agreement with the results published by the authors elsewhere (Bennion and Bachu, 2006b), which showed that displacement of brine by H_2S (lower IFT) resulted in higher residual brine saturations compared to displacement of brine by CO_2 (higher IFT).

In order to further investigate the effect of IFT on the brine recovery factor, as part of the experimental work conducted here, using two of the previously CO_2 flooded samples (BS-1-H and BS-2-H), two additional two-cycle (one drainage and one imbibition) experiments were carried out in which CO_2-saturated brine was displaced using methane instead of CO_2 and then during a subsequent imbibition cycle the samples were flooded by CO_2-saturated brine. As was expected, replacing the CO_2 by CH_4 improved the displacement performance during the drainage cycles through increasing the IFT, which in turn caused considerable reductions in the end-point residual brine saturation levels (Table 8). In accordance with the above discussion on the effect of IFT on breakthrough times, much of the enhanced brine recovery occurred for the methane injection case, by postponing the breakthrough time to times longer than those of CO_2 displacing the brine (Figs. 18 and 19). Lower residual brine saturations during CH_4 injection was achieved despite the fact that the viscosity of CH_4 was almost half that of supercritical CO_2 under the same conditions. It is worth noting that, since the brine used here was already fully saturated with CO_2 it was assumed that no more CH_4 would be dissolved in the brine during these two experiments and they could also be considered as pure immiscible displacements.

The required threshold pressure for the non-wetting phase to pass through a pore-throat is analogous to the initial threshold pressure for the non-wetting phase to enter a porous medium during capillary pressure measurement, which, if the porous medium remains the same, would be higher for fluid pairs with higher IFT and larger contact angle. The published experimental results by Hildenbrand et al. (2004) support the higher threshold pressure and subsequently occurrence of delayed breakthrough times for CH_4 injection compared to CO_2 injection. If wettability alteration due to CO_2 contact with a porous medium (Chiquet et al., 2007) is also considered to occur, difference in contact angle (θ) between the CO_2–brine and CH_4–brine systems also could influence the displacement. It is worth noting that, since the sandstone samples used were all considered to be strongly water-wet, without any wettability alterations, for both CO_2 and CH_4 displacements, contact angle is considered to be zero.

It should be noted that the effect of the IFT on the sweep efficiency during a drainage process would be most felt if the displacement suffers from a high mobility ratio. Otherwise, if the mobility ratio is less than one, in such processes, lowering or increasing the IFT is not expected to considerably change the residual wetting phase saturation.

Plotted in Fig. 20 are the end-point brine saturations obtained at the end of the first drainage cycle performed on various samples. As can be seen, the brine residual saturations for a number of the samples, do not fit well into the expected trend of being inversely proportional to the permeability of the samples. Even, considering the saturation data for the highest permeability samples, one may expect that for sufficiently high permeabilities the trend may level off or even become opposed to the expectations. Possible causes of this behaviour could be unstable displacement (excessively high displacement velocities) (Peters and Flock, 1981) or gravity segregation (Craig et al., 1957; Guo et al., 1991) or previously described non-uniform displacement dominated by high mobility ratio and low IFT, or any possible combination of these.

Unstable displacement may be excluded from the likely causes as it was investigated by flow-rate sensitivity analysis. Experiment 9 is a repeat of Experiment 8 carried out afterwards, through the normal cyclic flooding procedure explained elsewhere, while decreasing the CO_2 injection flow-rate from 300 cm^3/h to 120 cm^3/h and brine injection flow-rate from 200 cm^3/h to 100 cm^3/h. Both of these experiments were conducted on sample BS-2-H, which was a sample with a moderate permeability. As can be seen in the saturation data presented in Table 9, for the first drainage cycle, not only this change did not improve the sweep efficiency, which could have done through promoting,

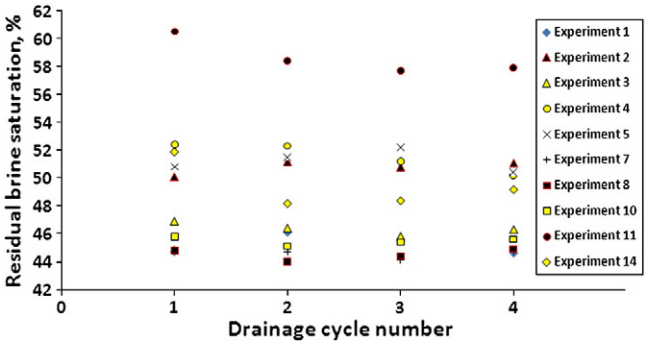

Fig. 17. Residual brine saturation data obtained at the end of all drainage cycles.

Table 8
Two additional drainage flooding experiments conducted on two of previously used samples using methane.

Test no.	Sample name	Pore vol, cm^3	k, mD	Overburden pressure, psi	Pore pressure, psi	Methane inj. flow-rate, cm^3/h	Capillary number, N_C	Endpoint S_w, %
15	BS-1-H	16.476	234.6	6725	2580	300	2.90E-06	29.4
16	BS-2-H	16.975	141.1	6725	2580	300	2.88E-06	35

presumably, a more stable displacement, but also reduced the brine recovery both at CO_2 breakthrough (BT) and at the end of the drainage cycles. The reduced brine recovery occurred because the coupled effect of high mobility ratio and low IFT became more pronounced in the case of low injection flow-rate, which in turn reduced the brine recovery by promoting a more non-uniform displacement. The same sensitivity analysis was performed once again on a low permeability sample (sample DB-1-H). Here the CO_2 injection flow-rate was increased to 200 cm^3/h from an original value of 150 cm^3/h and brine injection was increased from 100 cm^3/h to 150 cm^3/h. The higher flow-rate once again did not promote unstable displacement and even slightly improved the sweep efficiency. Here the difference between the end-point residual brine saturations achieved for the two scenarios was negligible because, as confirmed previously in the case of 150 cm^3/h CO_2 injection by conducting the "bump flow", the displacements were fairly uniform with minimum capillary interferences.

The effect of gravity segregation was systematically excluded from the experiments by placing the samples vertically inside the core-holder and performing the injections from base to the top. Therefore, the abnormal trend present among the saturation data measured for the samples with the higher permeabilities can only be attributed to the non-uniform displacement caused by the high mobility ratio, promoted by high viscosity contrast between the displaced and displacing fluids. This argument is also supported by the relatively small Capillary Numbers (N_c) (Eq. (1)) and Rapoport Scaling Coefficients (Eq. (2)) (Rapoport and Leas, 1953) calculated for each experiment and listed in Table 3. As already discussed, the presence of anomalous brine saturation caused by non-uniform displacement was also confirmed by conducting the "bump flows" at the end of the drainage cycles and by the first flow-rate sensitivity experiment. The highly non-uniform and rate dependence of displacement of brine by CO_2 was also confirmed through core-flooding simulations carried out by Shi et al. (2010).

$$N_c = \frac{\mu_1 \cdot u}{\sigma} \tag{1}$$

Where:

N_C	capillary number, *dimensionless*
μ_1	viscosity of the displacing fluid, Pa. s
u	superficial displacement velocity, m/s
σ	interfacial tension between the two fluids, N/m

$$\text{Scaling coefficient} = L \cdot u \cdot \mu \tag{2}$$

Where:

L	total length of the porous medium, cm
u	superficial displacement velocity, cm/s
μ	viscosity of the wetting phase, cP

Generally, Berea Sandstone samples had some of the lowest residual saturations among all, which could be attributed to their high degree of homogeneity coupled with their moderate permeability. The NMR T2 data generated for one of them (Fig. 21) also confirms that these samples benefit from a fairly homogeneous unimodal pore size distribution.

3.1.2. Imbibition cycles

The end-point residual CO_2 saturations obtained at the end of all three imbibition cycles conducted on all the samples are presented in Fig. 22. Similar to the brine residual saturations discussed before,

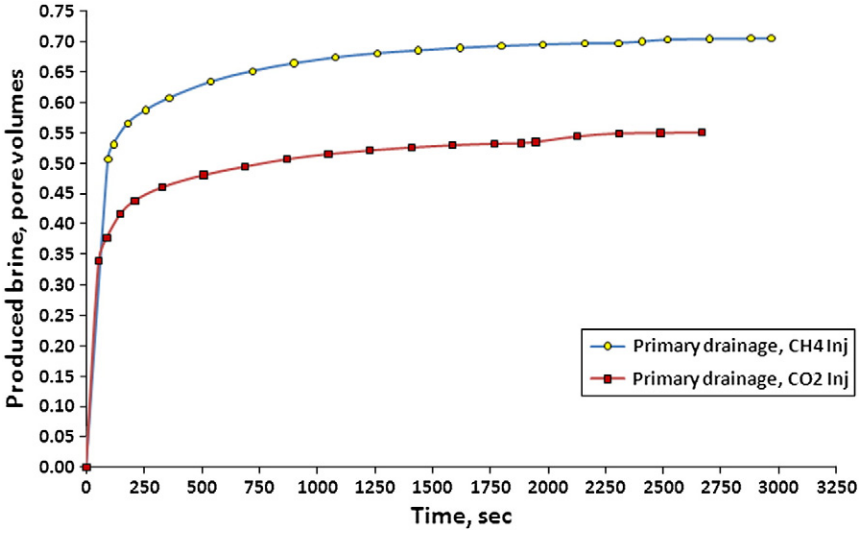

Fig. 18. Difference between the water production profiles during the primary drainage displacements conducted on sample BS-1-H using CH_4 and CO_2.

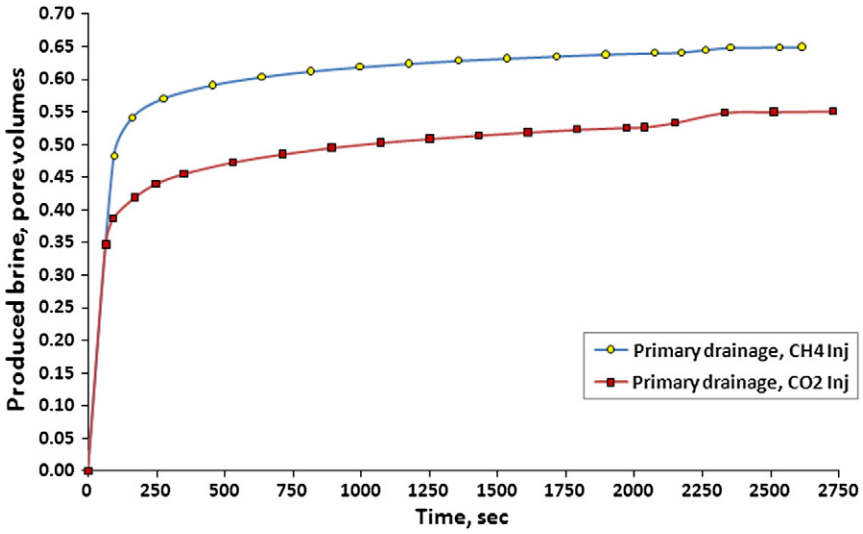

Fig. 19. Difference between the water production profiles during the primary drainage displacements conducted on sample BS-2-H using CH_4 and CO_2.

apart from a number of slight variations, there is no significant trend present among the data plotted in Fig. 22, which can possibly be used to support any possible effect of the cyclic flooding on the saturation profiles. However, if the saturation data resulted from the first imbibition cycles performed on various samples are analysed alone, there seems to be an excellent correlation between the residual CO_2 saturations and the permeability of the samples (Fig. 23). As one may expect, the residual saturation decreases with increase in the sample permeability. Unlike the trend found among the residual brine saturations, the trend found here remains consistent across the whole range of permeability values. This can be interpreted as a sign that displacement during the imbibition cycles was a uniform displacement without any major capillary interference. This is not something unexpected since considering the large contrast between the viscosities of brine and CO_2 under the experimental conditions applied here, the displacement of CO_2 by brine benefits from a very low mobility ratio.

As evident from the residual saturation data obtained at the end of the imbibition cycles conducted during the cyclic CO_2–brine injections (Table 4), one important feature of such displacement processes is their relatively low residual CO_2 saturation levels compared to those obtained when other common gases e.g. natural gas, are displaced by brine. As mentioned before two of the previously CO_2 flooded samples (BS-1-H and BS-2-H) were flooded for a second time with replacing the CO_2 by CH_4. The results of the primary drainage cycle (CH_4 displacing the brine) were discussed earlier. The end-point residual CH_4 saturations resulted from subsequent imbibition cycles performed on these two samples are presented in Table 10. As can be seen, the residual CH_4 saturations were considerably greater than those of CO_2 displaced by the same brine for the same samples. This difference in residual non-wetting phase saturation could be explained using the snap-off trapping mechanism and the difference in IFT between the two fluid systems.

With brine being the wetting phase and CO_2 or CH_4 the non-wetting phase, the residual trapping of CO_2 or CH_4 in the pore space would occur as a result of pore scale capillary pressure forces (Jerauld and Salter, 1990; Holtz, 2002). Generally there are three trapping models, namely pore-doublet, dead-end and snap-off models (Dullien, 1992; Holtz, 2002), which could be used to describe how the trapping of the non-wetting phase occurs during an imbibition process. In such imbibition processes as those conducted here the dominant trapping mechanism is snap-off (Piri et al., 2005; Al Mansoori, 2009; Knackstedt et al., 2010). The amount of the non-wetting phase trapped as a result of the snap-off depends on the aspect ratio of the pore channels and the IFT of the fluid system present inside the pores. Therefore, for the case of CO_2–brine system, due to the lower IFT between the two fluids, it can be expected to have lower trapped residual CO_2 saturations. This is exactly what the residual saturation data resulting from the imbibition cycles have shown during this experimental work.

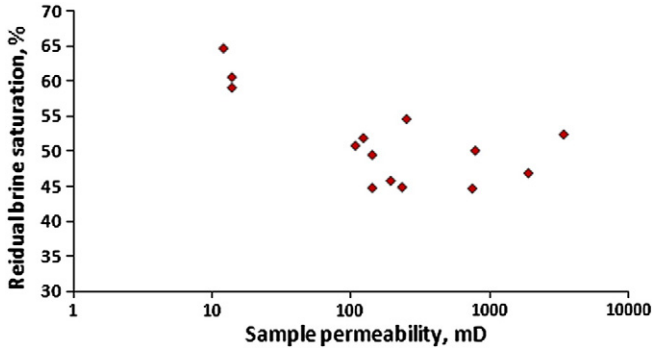

Fig. 20. Residual brine saturation values at the end of the first drainage cycle for all 14 CO_2 flooding experiments conducted.

Table 9
The results of flow-rate sensitivity analysis performed on two samples.

Test no.	Sample ID	k, mD	CO_2 flow-rate, cm^3/h	Pore volume brine produced before BT, %	End point residual brine saturation, %
8	BS-2-H	141.1	300	34.7	44.8
9	BS-2-H	141.1	120	31.6	49.5
11	DB-1-H	14	150	27.4	60.5
12	DB-1-H	14	200	28.0	59.0

The above conclusion is not the best outcome for those CO_2 geo-sequestration projects in which the main aim would be to sequester the injected CO_2 through residual capillary trapping. The situation worsens when the CO_2 is to be injected into high permeability formations. This type of formation normally suffer less from injectivity issues and since they are also expected to have high porosity values, they may have the advantage of presenting large capacities for CO_2 storage, but, at the same time, they offer an ultimate CO_2 entrapment, in the form of desired residual capillary trapping, far less than intermediate or less permeable formations. The lesser the CO_2 capillary entrapment is, the more CO_2 would remain as a free and movable phase which would eventually migrate upwards. This could be a major problem for storage sites without a comprehensive seal and for those with good confinement would mean more free CO_2 accumulation below the seal, which increases the risk of leakage or seal failure.

In high permeability formations, the already low amount of trapped residual CO_2 could reduce further when it is coupled with abnormally high residual brine saturations, which is likely to result due to high mobility ratio and low IFT, during the displacement of brine by the injected CO_2. Since less brine is displaced during a drainage cycle, less CO_2 would be available to be potentially trapped as a residual phase during a subsequent imbibition process. This is in agreement with the "Land" trapping model (Land, 1968), which relates the trapped residual non-wetting phase during an imbibition process to the maximum non-wetting phase saturation achieved at the end of the preceding drainage cycle.

3.2. Effect of cyclic CO_2–brine flooding on the differential pressure profiles

Despite the fact that for the case of cyclic CO_2–brine injection, there could not be found any significant relationship between the saturation data from one cycle to the next, the data obtained for the differential pressure across the sample show moderate to strong dependence on the cyclic flooding pattern. As evident from Figs. 7 to 12 the pressure data obtained during both drainage and imbibition cycles show similar trends. Therefore, unlike the saturation data, the two collections of pressure data generated (one for drainage and another for imbibition) will be analysed and discussed together.

One important point which needs to be mentioned with regards to the reported pressure data is that any data with a value less than 2 psi is outside the accuracy of the pressure sensors used. Therefore, for the high permeability samples e.g. CO2CRC-2,3-H, part of the measured differential pressure profiles fall outside the accuracy of the pressure transducers and for the moderate permeability samples, apart from the low end-point pressures, the reported differential pressure profiles for the individual injection cycles were reliable in terms of accuracy.

The normalised differential pressures across the sample at a point in time just before CO_2 breakthrough (BT) for drainage cycles performed on various samples are plotted in Fig. 24. The differential pressure values for each sample are normalised by dividing them by the differential pressure for the first cycle for that sample. As can be seen from the graph, there seems to be a moderate trend present among the data. The apparent general trend shows increase in the differential pressure from the first cycle to the last. This increase, however, seems to tend to level off with increasing the number of cycles. A large portion of the data plotted in Fig. 24 are for moderate to high permeability samples and as evident from the graph, despite the existence of a reasonable trend among the data for these samples, they also suffer from a number of uncorrelated fluctuations. As already pointed out, the main reason for this behaviour is the fact that the differential pressure values for these samples were small and the accuracy issue explained earlier dominated some of the measured data. One other possible cause of any uncorrelated fluctuation, as discussed in detail previously, could be non-uniform displacement of brine caused by high mobility ratio.

For the majority of the samples tested, the moderate trend observed among the data reported in Fig. 24 starts to diminish after CO_2 breakthrough as each drainage cycle approaches its completion.

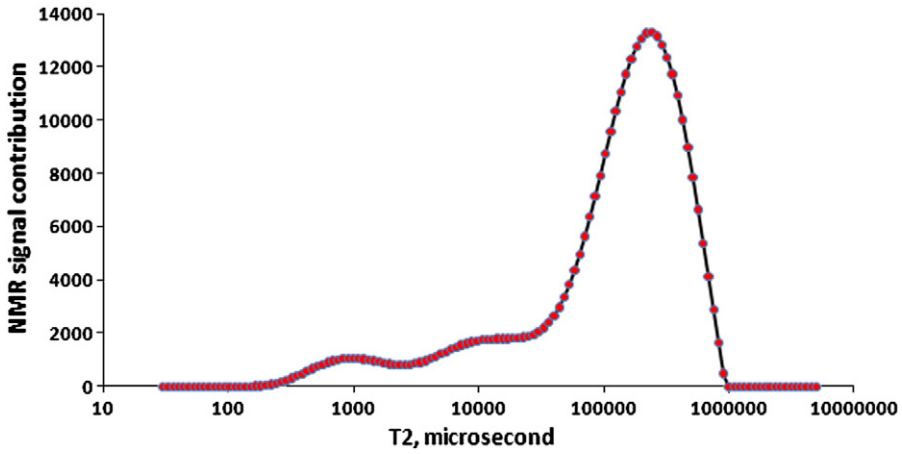

Fig. 21. Incremental T2 distribution for sample BS-1-H.

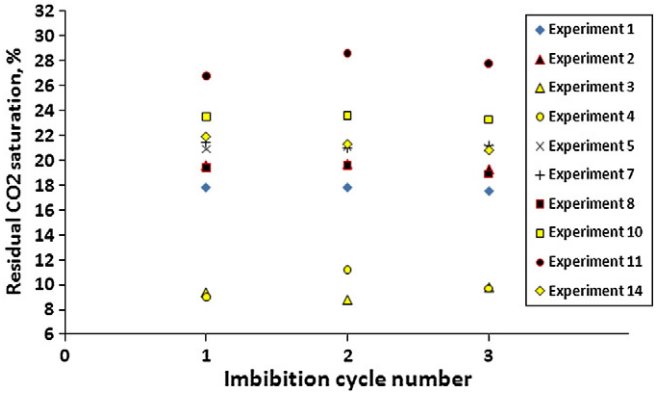

Fig. 22. End-point residual CO_2 saturations for all the imbibition cycles performed on various samples.

This is demonstrated by plotting those data in Fig. 25 for the end of the drainage cycles. As can be seen from this graph, except for a few samples, including sample DB-1-H, which is the lowest permeable sample, the rest of the data do not show any significant trend, which could be used to relate the change in the differential pressure profiles from one cycle to the next to the cyclic injection pattern. The likely cause of deviation from the original observed trend could be the fact that, first of all, towards the conclusion of each drainage cycle, the magnitude of the differential pressures become smaller and smaller until they stabilise and this makes the accuracy of the measured data worse towards the end of each cycle. Secondly, the recorded data after the CO_2 breakthrough are strongly affected by non-uniform capillary dominated displacement. If the after breakthrough data could be corrected for the negative effects of these influencing factors, very likely, they would also show trends similar to those observed among the data for before CO_2 breakthrough.

A similar trend to the one observed among the differential pressure data for the drainage cycles can also be seen among the data reported in Figs. 11 and 12 for the imbibition cycles performed on two samples. The trend which exists among the imbibition data however, is persistent for almost all the data after brine breakthrough. This could be attributed to the fact that, unlike the drainage cycles, imbibition floods did not suffer from negative impacts of unfavourable mobility ratio. Therefore, the imbibition displacements were fairly uniform all over. The viscosity of the displacing phase was also more than 10 times higher, which made the differential pressure during the imbibition cycles to be larger in magnitude and less prone to measurement in-accuracies. The other parameter, which confirms the existence of a uniform displacement during the imbibition cycles, is the brine breakthrough time which, unlike the slightly fluctuating breakthrough times for the drainage cycles, remained almost the same from one imbibition cycle to the next for each sample tested. During the following discussion it has been tried to find the most likely causes of the trends observed among the differential pressure data and see how these trends could be related to the cyclic flooding pattern.

From the data plotted in Figs. 24 and 25, the general conclusion was that with each consecutive injection cycle the pressure drop within the porous medium increases, however, it tends to level off gradually. One possible cause of such behaviour could be any formation damage which may occur inside the pore space due to the migration of fines, which could fully or partially plug or bridge the pore-throats. These fines are expected to be mainly dislodged clay particles within the samples or tiny particles inside the injection fluids pumped into the core samples. As described in the experimental procedure, the possibility of the presence of any particle in the injection fluids was eliminated by using a 0.5 μm sintered stainless steel high pressure in-line filter. With regards to clay particles, the majority of the samples used were of fairly clean sand e.g. Berea Sandstone and the samples from the Naylor Field. The type of clay in sample CL-40,68-H, which contained high clay content, was glauconite. Generally, glauconite, because of its relatively large particle sizes, does not tend to produce such fines that can be released into the pore space and cause formation damage. The only samples which could be prone to fines migration were DB-1-H and DB-2-V, which contained kaolinite. Although, overall, existing evidences show that for majority of the samples, damage to the samples due to fines migration may not be the main cause of the observed trend among the pressure data but it also may not be totally excluded from the equation at least for samples DB-1-H and DB-2-V.

The other possible cause of the observed trend among the differential pressure data could be the potential reactions between the slightly acidic brine, having CO_2 in solution, and a number of

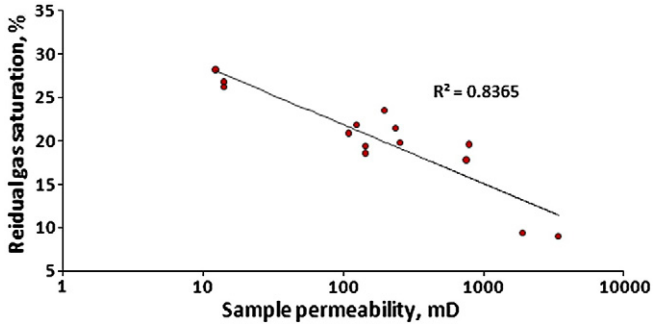

Fig. 23. Residual CO_2 saturation versus sample permeability.

Table 10
Two additional imbibition flooding experiments conducted on two of previously used samples using CO_2-saturated brine to displace methane.

Test no.	Sample name	Pore vol, cc	k, mD	Overburden pressure, psi	Pore pressure, psi	Brine inj. flow-rate, cm^3/h	Endpoint S_w, %
15	BS-1-H	16.476	234.6	6725	2580	200	68.0
16	BS-2-H	16.975	141.1	6725	2580	200	67.6

minerals inside the pore space of the samples (Eqs. (3) to (7)). These minerals include mainly calcite and dolomite, which exist in a number of samples mainly as the cement bounding the grains together and also making up a small fraction of the grains. The net effect of the possible dissolution and precipitation of these minerals could change the samples properties (Ross et al., 1982; Omole and Osoba, 1983; Sayegh et al., 1987; Bowker and Shuler, 1991; Shiraki and Dunn, 2000; Wellman et al., 2003; Grigg and Svec, 2006; Izgec et al., 2008) and even the strength of the samples to withstand the reservoir's in-situ net effective pressure. Using the results of the brine composition analyses (Table 6), it can be confirmed that mineral dissolution occurred during the experiments conducted. The occurrence of mineral precipitation could only be confirmed using appropriate techniques — such as SEM (Scanning Electron Microscopy). This type of analysis was not performed as part of this research but based on the available reports in the literature, the material dissolved in brine can subsequently precipitate in various forms and cause another type of formation damage. Based on the analyses performed and the information presented in the literature, occurrence of mineral precipitation possibly could have occurred during the experiments carried out, which may have caused damage to the sample pore space and subsequent changes in the differential pressure profiles from one cycle to the next.

$$CO_2 + H_2O_{(l)} \leftrightarrow H_2CO_{3(aq)} \leftrightarrow H^+_{(aq)} + HCO_3^-(aq) \quad (3)$$

$$\text{Silicates} + 2H^+ \leftrightarrow M^{2+} + \text{silica} \quad (4)$$

$$Mg^{2+}_{(aq)} + HCO_3^- \leftrightarrow H^+_{(aq)} + MgCO_{3(s)}(\text{magnesite}) \quad (5)$$

$$Ca^{2+}_{(aq)} + HCO^-_{3(aq)} \leftrightarrow H^+_{(aq)} + CaCO_{3(s)}(\text{calcite}) \quad (6)$$

$$Fe^{2+}_{(aq)} + HCO^-_{3(aq)} \leftrightarrow H^+_{(aq)} + FeCO_{3(s)}(\text{siderite}) \quad (7)$$

where:

M^{2+}	generic cation
l	liquid
aq	aqueous
s	solid

One more likely cause of change in the differential pressure profiles could be gradual physical compaction (creep) of the core samples during the extended cyclic floodings. This could occur in both high and low permeability samples but its relative impact is most felt by low porosity and permeability samples (Hall, 1953; Unalmiser and Swalwell, 1993), which, in most cases, would originally have the narrowest pore channels. Based on the dimension and porosity measurements performed on a number of the samples after they underwent the cyclic floodings (Table 5), it was confirmed that indeed core samples, to some degree, had undergone irreversible plastic compaction. Furthermore, using the results of the NMR measurements conducted on a number of the samples before and after the flooding experiments, a slight reduction in the total pore volume of the samples was detected. Figs. 13 and 14 are the incremental and cumulative T2 distribution for samples CO2CRC-2-H and CO2CRC-3-H, which were stacked together to make up composite sample CO2CRC-2,3-H. Fig. 15 also presents the same data for sample DB-1-H. As can be seen from these graphs, overall, all of the incremental T2 distributions, representing the relative pore size distribution of the samples, are shifted to the left, towards smaller pore sizes. The cumulative total T2, which is a measure of the total pore volume of each sample, shows a reduction for all three samples after subjecting them to the cyclic injections. Since some of the samples had calcite or dolomite or both within their cement, the already discussed mineral dissolution, which was confirmed to have occurred during the injection cycles, could have enhanced the plastic deformation of the samples by weakening the bond between the grains. It is worth noting that, for the type of samples tested in this study, there is about 1% error involved in the generation of the T2 distributions presented in Figs. 13 to 15.

The last likely cause of the observed trend among the differential pressure data, at least for the first two drainage cycles, could be the saturation history or capillary hysteresis (Larsen and Skauge, 1995; Bennion et al., 1996; Juanes et al., 2006). During the first drainage cycle CO_2 displaces only brine and there is no non-wetting phase (CO_2) saturation present in the pores, however, during a subsequent drainage cycle, there would be a non-wetting phase saturation left behind from the preceding imbibition cycle. As discussed before, since during an imbibition cycle, the trapped residual non-wetting phase saturation normally, due to the

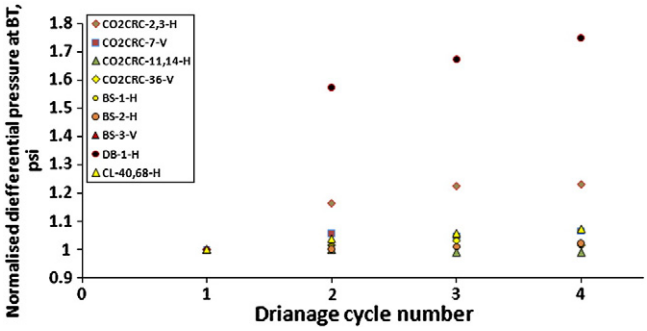

Fig. 24. Normalised differential pressures across the samples at a time just before CO_2 breakthrough (BT) for the drainage cycles.

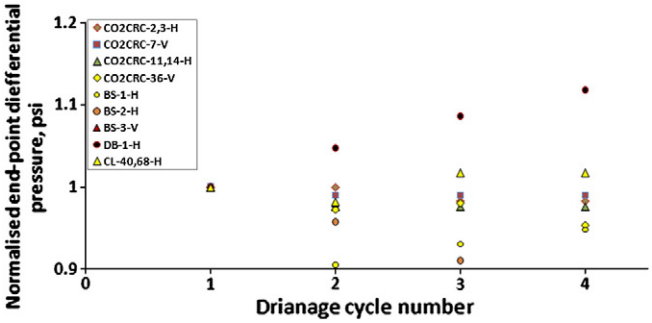

Fig. 25. Normalised end-point differential pressures across the samples at the end of the drainage cycles.

dominant snap-off mechanism, is left behind in pore bodies in the form of blobs and ganglia, it can put sever restriction on the flow of the wetting phase during a subsequent drainage cycle when it is being displaced by the non-wetting phase and this can create larger differential pressures across the porous medium. For the majority of the samples, as evident from the relatively large jump in the differential pressure from the first drainage cycle to the second one (Figs. 7 to 10), the effect of saturation history is mostly pronounced in the first two drainage cycles. After the second drainage, both saturation and differential pressure data do not show appreciable changes from one cycle to the other, therefore, the impact of the saturation history, would be minimal on the subsequent drainage cycles.

The observed trend among the differential pressure data (increase at the beginning followed by gradual stabilisation) is a characteristic of all four main possible causes discussed i.e. fines migration, mineral dissolution/precipitation, plastic compaction and saturation history. However, as pointed out earlier, fines migration could be reasonably ruled out as the main cause of this behaviour for the majority of the experiments. The existing experimental evidences show that plastic compaction, possibly enhanced by dissolution of the cements bounding the sandstone grains together, and the hysteresis effect have been the most influencing factors.

Sample CO2CRC-2-H was used upstream of sample CO2CRC-3-H within the composite sample including both. The NMR analysis was performed on these two short core-plugs separately with the hope of finding any effect of flow direction on the possible changes which may occur in the samples, but overall, the detected changes, at least with respect to their magnitude, are almost the same for both and there were no significant differences found between the two which could be possibly related to the direction of the fluid flow.

If the plotted pressure drop profiles in Figs. 7 to 12 are studied more closely, it can be seen that, for many of the samples tested, the pressure profiles become slightly less concave from the first injection cycle towards the last one. A less concave pressure profile is commonly a characteristic of low permeability core samples. Therefore, observing such behaviour supports the possibility of reduction in the pore and pore-throat sizes, which was confirmed to be the case by the results of the NMR measurements.

Based on the discussion presented on the effect of the cyclic flooding pattern on the differential pressure profiles across the samples, one may predict that the pressure drop within a porous medium subjected to the cyclic flooding of CO_2 and brine to increase gradually as further injection cycles are performed. Although, this increase is expected to level off after finite number of injection cycles. The results obtained here, apart from other various parts of the reservoir which may undergo cyclic flooding, have special application to the area around the wellbore. Any damage to this part of the reservoir due to any of the mechanisms discussed earlier i.e. fines migration, dissolution and subsequent precipitation of minerals, pore-space compaction enhanced by dissolution of the cement and weakening of the rock, hysteresis effect, etc., would eventually result in the reduction, or in extreme cases, loss of injectivity. It is worth noting that any damage caused by pore-space compaction could become less significant as the reservoir pore pressure increases with further CO_2 injection reducing the net effective pressure applied to the storage medium. It needs to be mentioned that the cyclic injection of CO_2 and brine may not always cause damage to the formation. Under favourable conditions the opposite could be possible too. However, among the possible interactions between the fluids and the rock, the only one which may cause enhancement to the formation is mineral dissolution.

4. Conclusion

The main conclusions arising from this experimental study are as follows:

1. *General displacement of brine by CO_2 or vice versa:*

- Overall, the residual brine saturations are abnormally high during displacement of wetting brine phase by non-wetting CO_2 phase. These abnormally high end-point residual brine saturations, especially in moderate to high permeability porous media, could be attributed to the combined effects of high mobility ratios and low IFT values dominating such drainage processes. This type of displacement is strongly flow-rate dependant.
- Unlike imbibition displacements conducted during EOR processes, during displacement of the wetting brine phase by a low viscosity non-wetting phase e.g. CO_2, natural gas, etc., (a drainage process dominated by high mobility ratio) reduction of the IFT makes the displacement process less effective in terms of brine sweep efficiency. This contradicts a common belief among many researchers to date.
- Overall, the residual CO_2 saturations during displacement of CO_2 by brine are relatively low. The low residual trapped CO_2 levels could be attributed to low IFT of the supercritical CO_2–brine system, which reduce the significance of the snap-off trapping mechanism as the main active capillary trapping mechanism during CO_2 geo-sequestration.
- The residual CO_2 trapping in high permeability porous media is expected to be low for two main reasons: First, the displacement

of CO_2 by brine in such formations is very efficient. Second, based on the "Land" trapping model, low obtainable maximum CO_2 saturations during a drainage cycle in such porous media subsequently results in low levels of trapped CO_2 during a subsequent imbibition cycle.

- Therefore, while CO_2 injectivity is expected to be high in highly permeable formations, the extremely low levels of CO_2 entrapment in the form of the desired residual saturation may make them less favourable for CO_2 storage purposes especially in a system lacking a comprehensive seal.

2. *Cyclic CO_2–brine flooding:*

- Overall, in low permeability samples, while the end-point saturations (for both drainage and imbibition) are expected to remain steady during a cyclic/alternating flooding pattern, pressure profiles and as a result the end-point relative permeabilities may show moderate to strong dependence on the cyclic/alternating injection pattern. However, any observed trend would weaken as the permeability of the porous medium increases.
- In low permeability samples and samples susceptible to formation damage e.g. fines migration, mineral dissolution/precipitation, etc., the injectivity, may decrease as the cyclic CO_2–brine injection proceeds. However, it is likely that the extent of any damage would stabilise after several injection cycles.
- During an extended cyclic CO_2–brine flooding of a porous medium, it is likely that the storage medium would undergo some degree of irreversible plastic deformation. The most likely cause of such deformation is the dissolution of some minerals present in the cement bounding the rock grains together. Dissolution of the cement would weaken this bound and intensify the plastic compaction of the porous medium. Although, over time, increase in the reservoir pore pressure could slow down the compaction process by reducing the net effective pressure applied to the storage medium.
- Capillary hysteresis effect can have moderate to strong effects on the injectivity during underground cyclic CO_2–brine injection, however, its effect is expected to be limited mainly to the first and second flooding cycles.

The samples used during this study were all sandstone. Considering the potentially higher degree of interactions between the carbonate samples and the fluids involved, conducting core-flooding tests such as those performed here using carbonate samples could potentially yield more interesting results. Therefore, in order to fully understand the nature of the multiphase flow characteristics of the rock–fluids system during cyclic CO_2–brine flooding, pertaining to all types of target storage media, a similar study involving carbonate samples is necessary.

Acknowledgment

This work was supported in part by funds from Cooperative Research Centre for Greenhouse Gas Technologies (CO2CRC). We would like to thank CO2CRC's management for their financial support during the course of development of this research. We also would like to thank Dr. Lincoln Paterson from CSIRO for all the useful discussions.

References

Al Mansoori, S.K., 2009. Impact of carbon dioxide trapping on geological storage. PhD Thesis, Imperial College, London, 197 pp.

Bennion, B., Bachu, S., 2005. Relative permeability characteristics for supercritical CO_2 displacing water in a veriety of potential sequestration zones in the Western Canada sedimentary basin, SPE 95547. The SPE Annual Technical Conference and Exhibition. Society of Petroleum Engineers, Dallas, Texas, USA.

Bennion, B., Bachu, S., 2006a. Dependence on temperature, pressure, and salinity of the IFT and relative permeability displacement characteristics of CO_2 injected in deep saline aquifers, SPE 102138. SPE Annual Technical Conference and Exhibition. Society of Petroleum Engineers, San Antonio, Texas, USA.

Bennion, B., Bachu, S., 2006b. Supercritical CO_2 and H_2S–brine drainage and imbibition relative permeability relationships for intergranular sandstone and carbonate formations, SPE 99326. SPE Europec/EAGE Annual Conference and Exhibition. Society of Petroleum Engineers, Vienna, Austria.

Bennion, B., Bachu, S., 2007. Permeability and relative permeability measurements at reservoir conditions for CO_2–water systems in ultra low permeability confining caprocks. SPE 106995, EUROPEC/EAGE Conference and Exhibition. Society of Petroleum Engineers, London, U.K.

Bennion, B., Bachu, S., 2010. Drainage and imbibition CO_2/brine relative permeability curves at reservoir conditions for carbonate formations. SPE 134028 SPE Annual Technical Conference and Exhibition. Society of Petroleum Engineers, Florence, Italy.

Bennion, B., Thomas, F.B., Bietz, R.F., 1996. The Effect of Trapped Critical Fluid Saturations on Reservoir Permeability and Conformance. Hycal Energy Research Laboratories Ltd.

Bowker, K.A., Shuler, P.J., 1991. Carbon dioxide injection and resultant alteration of the Weber Sandstone, Rangely Field, Colorado. AAPG Bull. 75 (9), 1489–1499.

Chiquet, P., Broseta, D., Thibeau, S., 2007. Wettability alteration of caprock minerals by carbon dioxide. Geofluids 7 (2), 112–122.

Coates, G.R., Xiao, L., Prammer, M.G., 1999. NMR Logging — Principles & Applications. Halliburton Energy Services, Houston.

Craig, F.F., 1975. The Reservoir Engineering Aspects of Waterflooding SPE Monograph Series 3. Society of Petroleum Engineers, Dallas, Texas.

Craig, F.F.J., Sanderlin, J.L., Moore, D.W., Geffen, T.M., 1957. A laboratory study of gravity segregation in frontal drives. SPE 676-G. Petrol. Trans. AIME 210, 275–282.

Doughty, C., Pruess, K., 2004. Modeling supercritical carbon dioxide injection in heterogeneous porous media. Vadose Zone Journal 3 (3), 837–847.

Dullien, F.A.L., 1992. Porous Media: Fluid Transport and Pore Structure. Academic Press, New York.

Emeka Eke, P., Curtis, A., Haszeldine, S., 2009. CO_2–brine surface dissolution and injection: CO_2 storage enhancement. SPE 124711, Offshore Europe. Society of Petroleum Engineers, Aberdeen, UK.

Espinoza, D.N., Santamarina, J.C., 2010. Water–CO_2–mineral systems: interfacial tension, contact angle, and diffusion—implications to CO_2 geological storage. Water Resour. Res. 46 (7), W07537.

Grigg, R.B., Svec, R.K., 2006. CO_2 transport mechanisms in CO_2/brine coreflooding, SPE 103228. SPE Annual Technical Conference and Exhibition. Society of Petroleum Engineers, San Antonio, Texas, USA.

Guo, Y., Nilsen, V., Hovland, F., 1991. Gravity effect under steady-state and unsteady-state core flooding and criteria to avoid it. The Second Society of Core Analysts European Core Analysis Symposium London, UK.

Hall, H.N., 1953. Compressibility of reservoir rocks. SPE 953309. Petrol. Trans. AIME 198, 309–311.

Heaviside, J., Black, C.J.J., 1983. Fundamentals of relative permeability: experimental and theoretical considerations, SPE 12173. SPE Annual Technical Conference and Exhibition. Society of Petroleum Engineers of AIME, San Francisco, California.

Hildenbrand, A., Schlömer, S., Krooss, B.M., Littke, R., 2004. Gas breakthrough experiments on pelitic rocks: comparative study with N_2, CO_2 and CH_4. Geofluids 4 (1), 61–80.

Hinkley, R.E., Davis, L.A., 1986. Capillary pressure discontinuities and end effects in homogeneous composite cores: effect of flow rate and wettability, SPE 15596. 1986 Copyright 1986 SPE Annual Technical Conference and Exhibition. Society of Petroleum Engineers, Inc, New Orleans, Louisiana.

Holtz, M.H., 2002. Residual gas saturation to aquifer influx: a calculation method for 3-D computer reservoir model construction, SPE 75502. Copyright 2002 SPE Gas Technology Symposium. Society of Petroleum Engineers Inc, Calgary, Alberta, Canada.

Izgec, O., Demiral, B., Bertin, H., Akin, S., 2008. CO_2 injection into saline carbonate aquifer formations I: laboratory investigation. Transp. Porous Media 72 (1), 1–24.

Jerauld, G.R., Salter, S.J., 1990. The effect of pore-structure on hysteresis in relative permeability and capillary pressure: pore-level modeling. Transp. Porous Media 5 (2), 103–151.

Juanes, R., Spiteri, E.J., Orr Jr., F.M., Blunt, M.J., 2006. Impact of relative permeability hysteresis on geological CO_2 storage. Water Resour. Res. 42, W12418.

Knackstedt, M.A., Dance, T., Kumar, M., Averdunk, H., Paterson, L., 2010. Enumerating permeability, surface areas, and residual capillary trapping of CO_2 in 3D: digital analysis of CO2CRC Otway Project core, SPE 134625. SPE Annual Technical Conference and Exhibition. Society of Petroleum Engineers, Florence, Italy.

Kumar, A., et al., 2005. Reservoir simulation of CO2 storage in deep saline aquifers. SPE 89343, SPE Journal 10 (3), 336–348.

Land, C.S., 1968. Calculation of imbibition relative permeability for two- and three-phase flow from rock properties SPE 1942 SPE J. 8 (2), 149–156.

Langaas, K., Ekrann, S., Ebeltoft, E., 1998. A criterion for ordering individuals in a composite core. J. Pet. Sci. Eng. 19 (1–2), 21–32.

Larsen, J.A., Skauge, A., 1995. Comparing hysteresis models for relative permeability in WAG studies. 1995 SCA Conference, Paper number 9506.

Leet, L.D., Judson, S., 1971. Physical Geology. Prentice-Hall, Englewood Cliffs, New Jersey.

Nordbotten, J.M., Celia, M.A., Bachu, S., 2005. Injection and storage of CO2 in deep saline aquifers: analytical solution for CO2 plume evolution during injection. Transport in Porous Media 58 (3), 339–360.

Omole, O., Osoba, J.S., 1983. Carbon dioxide — dolomite rock interaction during CO_2 flooding process. Annual Technical Meeting. Petroleum Society of Canada, Banff.
Osoba, J.S., Richardson, J.G., Kerver, J.K., Hafford, J.A., Blair, P.M., 1951. Laboratory measurements of relative permeability. SPE 951047. Petrol. Trans. AIME 192, 47–56.
Perrin, J.-C., et al., 2009. Core-scale experimental study of relative permeability properties of CO_2 and brine in reservoir rocks. Energy Procedia 1 (1), 3515–3522.
Peters, E.J., Flock, D.L., 1981. The onset of instability during two-phase immiscible displacement in porous media. SPE 8371. SPE J. 21 (2), 249–258.
Piri, M., Prévost, J.H., Fuller, R., 2005. Carbon dioxide sequestration in saline aquifers: evaporation, precipitation and compressibility effects. Fourth Annual Conference on Carbon Capture and Sequestration. Alexandria, Virginia.
Pope, G.A., Baviere, M., 1991. Basic Concepts in Enhanced Oil Recovery Processes. In: Baviere, M. (Ed.), Elsevier Applied Science, London.
Rapoport, L.A., Leas, W.J., 1953. Properties of linear waterfloods. SPE 213-G. Petrol. Trans. AIME 198, 139–148.
Ross, G.D., Todd, A.C., Tweedie, J.A., Will, A.G., 1982. The dissolution effects of CO_2–brine systems on the permeability of U.K. and North Sea calcareous sandstones. SPE 10685, SPE/DOE Third Joint Symposium on Enhanced Oil Recovery of the Society of Petroleum Engineers. Society of Petroleum Engineers, Tulsa, OK.
Sayegh, S.G., Krause, F.F., Girard, M., Debree, C., 1987. Rock-carbonated brine interactions: Part I. Cardium formation cores. Annual Technical Meeting. Petroleum Society of Canada, Calgary, Alberta.
Sharma, S., Cook, P., Berly, T., Lees, M., 2009. The CO2CRC Otway Project: overcoming challenges from planning to execution of Australia's first CCS project. Energy Procedia 1 (1), 1965–1972.
Shi, J.-Q., Xue, Z., Durucan, S., 2010. Supercritical CO2 core flooding and imbibition in Tako sandstone-Influence of sub-core scale heterogeneity. International Journal of Greenhouse Gas Control 5 (1), 75–87.
Shiraki, R., Dunn, T.L., 2000. Experimental study on water–rock interactions during CO_2 flooding in the Tensleep Formation, Wyoming, USA. Appl. Geochem. 15 (3), 265–279.
Spencer, L., Xu, Q., LaPedalina, F., Weir, G., 2006. Site characterization of the Otway Basin Storage Pilot in Australia. Proceeding of the 8th International Conference on Greenhouse Gas Control Technologies, Trondheim, Norway.
Unalmiser, S., Swalwell, T.J., 1993. A quick technique to define compressibility characteristics of hydrocarbon reservoir, SPE 25912. Low Permeability Reservoirs Symposium. Society of Petroleum Engineers, Denver, Colorado.
Wellman, T.P., Grigg, R.B., McPherson, B.J., Svec, R.K., Lichtner, P.C., 2003. Evaluation of CO_2–brine–reservoir rock interaction with laboratory flow tests and reactive transport modeling. International Symposium on Oilfield Chemistry. Society of Petroleum Engineers, Houston, Texas.
Zekri, A.Y., Almehaideb, R.A., 2006. Relative permeability measurements of composite cores — an experimen\tal approach. Pet. Sci. Technol. 24 (6), 717–736.